

A Neural Tangent Kernel Perspective of Infinite Tree Ensembles

Ryuichi Kanoh^{1,2}, Mahito Sugiyama^{1,2}

¹National Institute of Informatics

²The Graduate University for Advanced Studies, SOKENDAI
{kanoh, mahito}@nii.ac.jp

Abstract

In practical situations, the ensemble tree model is one of the most popular models along with neural networks. A *soft tree* is one of the variants of a decision tree. Instead of using a greedy method for searching splitting rules, the soft tree is trained using a gradient method in which the whole splitting operation is formulated in a differentiable form. Although ensembles of such soft trees have been increasingly used in recent years, little theoretical work has been done for understanding their behavior. In this paper, by considering an ensemble of *infinite* soft trees, we introduce and study the *Tree Neural Tangent Kernel* (TNTK), which provides new insights into the behavior of the infinite ensemble of soft trees. Using the TNTK, we succeed in theoretically finding several non-trivial properties, such as the effect of the oblivious tree structure and the degeneracy of the TNTK induced by the deepening of the trees. Moreover, we empirically examine the performance of an ensemble of infinite soft trees using the TNTK.

1 Introduction

Tree ensembles such as random forests (Breiman, 2001) are powerful machine learning models used in various real-world applications. Since finding optimal splits at different levels of a decision tree according to some global objective is known to be NP-complete (Hyafil & Rivest, 1976), trees are often constructed using a greedy method (Quinlan, 1986; Breiman et al., 1984). Instead of searching for hard splitting rules, one way to construct a non-greedy decision tree is to make the splitting rules *soft* and updating the entire model’s parameters simultaneously using the gradient method. Such soft trees are expected to be a good compromise as they inherit characteristics of both neural networks and decision trees. Soft tree ensemble models are known to have high empirical performance (Arik & Pfister, 2019; Popov et al., 2020; Kotschieder et al., 2015; Hazimeh et al., 2020), especially for tabular datasets. Besides accuracy, there are many additional reasons as to why one should formulate trees in a soft manner. For example, unlike hard decision trees, the model can be updated sequentially (Ke et al., 2019) and trained in combination with pre-training (Arik & Pfister, 2019), resulting in favorable characteristics in terms of real-world continuous service deployment. Their model interpretability induced by the hierarchical splitting structure has also attracted much attention (Frosst & Hinton, 2017; Wan et al., 2021; Tanno et al., 2019). In addition, the idea of the soft tree is implicitly used in many different places; for example, the process of allocating data to the appropriate leaves can be interpreted as a special case of Mixture-of-Experts (Jordan & Jacobs, 1993; Shazeer et al., 2017; Lepikhin et al., 2021), a technique for balancing computational complexity and prediction performance.

Although various techniques have been proposed to train trees, the theoretical validity of such techniques is not well understood at sufficient depth. To understand the training of tree ensemble models, we focus on the *Neural Tangent Kernel* (NTK) (Jacot et al., 2018; Lee et al., 2019), a powerful tool that has been successfully applied to various neural network models with *infinite* hidden layer nodes. Every model architecture is known to produce a distinct NTK. Not only for the

multi-layer perceptron (MLP), many studies have been performed across various models, such as for Convolutional Neural Networks (CNTK) (Arora et al., 2019b; Li et al., 2019), Graph Neural Networks (GNTK) (Du et al., 2019), and Recurrent Neural Networks (RNTK) (Alemohammad et al., 2021). However, it is not obvious how to apply the NTK theory to the tree models.

In this paper, by considering the limit of infinitely many trees, we introduce and study the neural tangent kernel for tree ensembles, called the *Tree Neural Tangent Kernel* (TNTK), which provides new insights into the behavior of the infinite ensemble of soft trees. Our contributions are summarized as follows:

- **First extension of the NTK concept to the tree ensemble models.** We derive the analytical form for the TNTK at initialization induced by infinitely many complete binary trees with arbitrary depth. The proof is based on the correspondence between the number of trees and the number of hidden layer nodes in the MLP, which we use to achieve applying the NTK theory to the soft tree ensembles for the first time (Section 4.1).
- **Equivalence of the oblivious tree ensemble models.** We show that the TNTK induced by the oblivious tree structure used in practical open-source libraries such as CatBoost (Prokhorenkova et al., 2018) and NODE (Popov et al., 2020) converges to the same TNTK induced by a non-oblivious one in the limit of infinite trees. This observation implicitly supports the good empirical performance of oblivious trees with parameter sharing between tree nodes (Section 4.1.1).
- **Degeneracy of the TNTK with deep trees.** The TNTK associated with deep trees exhibits degeneracy; the TNTK values are almost identical for deep trees even if the inner products of inputs are different. As a result, poor performance in numerical experiments is observed with the TNTK induced by infinitely many deep trees. This result supports the fact that the depth of trees is usually not so large in practical situations (Section 4.1.2).
- **Constant TNTK during training.** We prove that the TNTK remains constant during the training of infinite soft trees. This allows us to analyze the behavior by kernel regression and to discuss the global convergence of training using the positive definiteness of the TNTK. Although our framework based on soft trees allows us to consider hard trees by taking the infinitely large degree of hardness of tree splitting, it should be noted that the constantness no longer holds for such a case. Therefore, our theoretical discussion does not directly support hard decision trees (Section 4.1.3, 4.2).
- **Comparison to the NTK induced by the MLP.** We investigate the generalization performance of infinite tree ensembles by kernel regression with the TNTK on 90 real-world datasets. Although the MLP with infinite width has better prediction accuracy on average, the infinite tree ensemble performs better than the infinite width MLP in more than 30% of the datasets. We also showed that the TNTK is superior to the MLP-induced NTK in terms of computational speed (Section 5).

2 Background and related work

Our main focus in this paper is the soft tree and the neural tangent kernel. We briefly introduce and review them.

2.1 Soft tree

Based on Kotschieder et al. (2015), we formulate a regression by soft trees. Figure 1 is a schematic image of an ensemble of M soft trees. We define a data matrix $\mathbf{x} \in \mathbb{R}^{N_0 \times N}$ for N training samples $\{\mathbf{x}_1, \dots, \mathbf{x}_N\}$ with N_0 features and define tree-wise parameter matrices for internal nodes $\mathbf{w}_m \in \mathbb{R}^{N_0 \times \mathcal{N}}$ and leaf nodes $\boldsymbol{\pi}_m \in \mathbb{R}^{1 \times \mathcal{L}}$ for each tree $m \in [M] = \{1, \dots, M\}$ as

$$\mathbf{x} = \begin{pmatrix} | & \cdots & | \\ \mathbf{x}_1 & \cdots & \mathbf{x}_N \\ | & \cdots & | \end{pmatrix}, \quad \mathbf{w}_m = \begin{pmatrix} | & \cdots & | \\ \mathbf{w}_{m,1} & \cdots & \mathbf{w}_{m,\mathcal{N}} \\ | & \cdots & | \end{pmatrix}, \quad \boldsymbol{\pi}_m = (\pi_{m,1}, \dots, \pi_{m,\mathcal{L}}),$$

where internal nodes (blue nodes in Figure 1) and leaf nodes (green nodes in Figure 1) are indexed from 1 to \mathcal{N} and 1 to \mathcal{L} , respectively. \mathcal{N} and \mathcal{L} may change across trees in general, while we assume that they are always fixed for simplicity throughout the paper. We also write horizontal concatenation of (column) vectors as $\mathbf{x} = (\mathbf{x}_1, \dots, \mathbf{x}_N) \in \mathbb{R}^{N_0 \times N}$ and $\mathbf{w}_m = (\mathbf{w}_{m,1}, \dots, \mathbf{w}_{m,\mathcal{N}}) \in \mathbb{R}^{N_0 \times \mathcal{N}}$. Unlike hard decision trees, we consider a model in which every single leaf node $\ell \in [\mathcal{L}] = \{1, \dots, \mathcal{L}\}$

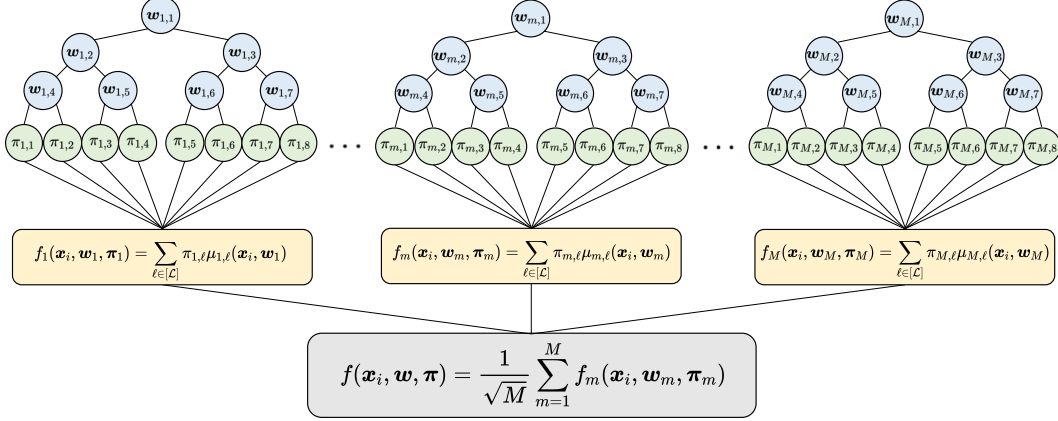


Figure 1: Schematics of an ensemble of M soft trees. Tree internal nodes are indexed according to the breadth-first ordering.

of a tree m holds the probability that data will reach to it. Therefore, splitting operation at an intermediate node $n \in [\mathcal{N}] = \{1, \dots, \mathcal{N}\}$ does not definitively decide splitting to the left or right.

To provide an explicit form of the probabilistic tree splitting operation, we introduce the following binary relations that depend on the tree's structure: $\ell \swarrow n$, which is true if a leaf ℓ belongs to the left subtree of a node n and false otherwise, and $n \searrow \ell$, which is true if a leaf ℓ belongs to the right subtree of a node n and false otherwise. We can now exploit $\mu_{m,\ell}(\mathbf{x}_i, \mathbf{w}_m) : \mathbb{R}^{N_0} \times \mathbb{R}^{N_0 \times \mathcal{N}} \rightarrow [0, 1]$, a function that returns the probability that a sample \mathbf{x}_i will reach a leaf ℓ of the tree m , as follows:

$$\mu_{m,\ell}(\mathbf{x}_i, \mathbf{w}_m) = \prod_{n=1}^{\mathcal{N}} g_{m,n}(\mathbf{x}_i, \mathbf{w}_{m,n})^{\mathbb{1}_{\ell \swarrow n}} (1 - g_{m,n}(\mathbf{x}_i, \mathbf{w}_{m,n}))^{\mathbb{1}_{n \searrow \ell}}, \quad (1)$$

where $\mathbb{1}_Q$ is an indicator function conditioned on the argument Q , i.e., $\mathbb{1}_{\text{true}} = 1$ and $\mathbb{1}_{\text{false}} = 0$, and $g_{m,n} : \mathbb{R}^{N_0} \times \mathbb{R}^{N_0} \rightarrow [0, 1]$ is a decision function at each internal node n of a tree m . To approximate decision tree splitting, the output of the decision function $g_{m,n}$ should be between 0.0 and 1.0. If the output of a decision function takes only 0.0 or 1.0, the splitting operation is equivalent to hard splitting used in typical decision trees. We will define an explicit form of the decision function $g_{m,n}$ in Equation (5) in the next section.

The prediction for each \mathbf{x}_i from a tree m with nodes parameterized by \mathbf{w}_m and $\boldsymbol{\pi}_m$ is given by

$$f_m(\mathbf{x}_i, \mathbf{w}_m, \boldsymbol{\pi}_m) = \sum_{\ell=1}^{\mathcal{L}} \pi_{m,\ell} \mu_{m,\ell}(\mathbf{x}_i, \mathbf{w}_m), \quad (2)$$

where $f_m : \mathbb{R}^{N_0} \times \mathbb{R}^{N_0 \times \mathcal{N}} \times \mathbb{R}^{1 \times \mathcal{L}} \rightarrow \mathbb{R}$, and $\pi_{m,\ell}$ denotes the response of a sample reaching a leaf ℓ of the tree m . This formulation means that the prediction output is the average of the leaf values $\pi_{m,\ell}$ weighted by $\mu_{m,\ell}(\mathbf{x}_i, \mathbf{w}_m)$, probability of assigning the sample \mathbf{x}_i to the leaf ℓ . If $\mu_{m,\ell}(\mathbf{x}_i, \mathbf{w}_m)$ takes only 1.0 for one leaf and 0.0 for the other leaves, the behavior is equivalent to a typical decision tree prediction. In this model, \mathbf{w}_m and $\boldsymbol{\pi}_m$ are updated during training with a gradient method.

While many empirical successes have been reported, theoretical analysis for soft tree ensemble models has not been sufficiently developed.

2.2 Neural Tangent Kernel

Given N samples $\{\mathbf{x}_1, \dots, \mathbf{x}_N\}$, the NTK induced by any model architecture at a training time τ is formulated as a matrix $\widehat{\mathbf{H}}_\tau^* \in \mathbb{R}^{N \times N}$, in which each $(i, j) \in [N] \times [N]$ component is defined as

$$[\widehat{\mathbf{H}}_\tau^*]_{ij} := \widehat{\Theta}_\tau^*(\mathbf{x}_i, \mathbf{x}_j) := \left\langle \frac{\partial f_{\text{arbitrary}}(\mathbf{x}_i, \boldsymbol{\theta}_\tau)}{\partial \boldsymbol{\theta}_\tau}, \frac{\partial f_{\text{arbitrary}}(\mathbf{x}_j, \boldsymbol{\theta}_\tau)}{\partial \boldsymbol{\theta}_\tau} \right\rangle, \quad (3)$$

where $\langle \cdot, \cdot \rangle$ denotes the inner product and $\theta_\tau \in \mathbb{R}^P$ is a concatenated vector of all the P trainable model parameters at τ . An asterisk “*” indicates that the model is arbitrary. The model function $f_{\text{arbitrary}} : \mathbb{R}^{N_0} \times \mathbb{R}^P \rightarrow \mathbb{R}$ used in Equation (3) is expected to be applicable to a variety of model structures. For the soft tree ensembles introduced in Section 2.1, the NTK is formulated as $\sum_{m=1}^M \sum_{n=1}^N \left\langle \frac{\partial f(\mathbf{x}_i, \mathbf{w}, \boldsymbol{\pi})}{\partial \mathbf{w}_{m,n}}, \frac{\partial f(\mathbf{x}_j, \mathbf{w}, \boldsymbol{\pi})}{\partial \mathbf{w}_{m,n}} \right\rangle + \sum_{m=1}^M \sum_{\ell=1}^L \left\langle \frac{\partial f(\mathbf{x}_i, \mathbf{w}, \boldsymbol{\pi})}{\partial \pi_{m,\ell}}, \frac{\partial f(\mathbf{x}_j, \mathbf{w}, \boldsymbol{\pi})}{\partial \pi_{m,\ell}} \right\rangle$.

In the limit of infinite width with a proper parameter scaling, a variety of properties have been discovered for the NTK induced by the MLP. For example, Jacot et al. (2018) showed the convergence of $\hat{\Theta}_0^{\text{MLP}}(\mathbf{x}_i, \mathbf{x}_j)$, which can vary with respect to parameters, to the unique limiting kernel $\Theta(\mathbf{x}_i, \mathbf{x}_j)$ at initialization in probability. Moreover, they also showed that the limiting kernel does not change during training in probability:

$$\lim_{\text{width} \rightarrow \infty} \hat{\Theta}_\tau^{\text{MLP}}(\mathbf{x}_i, \mathbf{x}_j) = \lim_{\text{width} \rightarrow \infty} \hat{\Theta}_0^{\text{MLP}}(\mathbf{x}_i, \mathbf{x}_j) =: \Theta^{\text{MLP}}(\mathbf{x}_i, \mathbf{x}_j). \quad (4)$$

This property helps in the analytical understanding of the model behavior. For example, with the squared loss and infinitesimal step size with learning rate η , the training dynamics of gradient flow in function space coincides with kernel ridge-less regression with the limiting NTK. In addition, if the NTK is positive definite, the training can achieve global convergence.

A number of insights into the model structure have been obtained through analysis using the NTK. Huang et al. (2020) show that while the NTK of simple MLPs degenerates as the layers become deep, models with skip-connection do not degenerate as seen in MLP, and explain why training of deep models works well with skip-connection. Alemohammad et al. (2021) analytically derived NTKs for the recurrent neural network (RNN) and showed that the introduction of weight-sharing, which is commonly used in RNN, does not change the NTK from models without weight-sharing, demonstrating the validity of the existing treatment. Li et al. (2019) showed the correspondence between pixel-shift based data augmentation and global average pooling operations commonly used with the convolutional neural network architecture, and developed discussions from previously unavailable perspectives.

The NTK theory is often used in the context of the overparameterization of neural networks. In response to recent trends, overparameterization is also a subject of interest for tree ensembles (Belkin et al., 2019; Karthikeyan et al., 2021). Although a number of findings have been obtained using the NTK, they are mainly for typical neural networks such as MLP and ResNet, and the NTK theory has not been applied to tree models yet.

3 Setup

We train model parameters \mathbf{w} and $\boldsymbol{\pi}$, where $\mathbf{w} = (\mathbf{w}_1, \dots, \mathbf{w}_m)$ and $\boldsymbol{\pi} = (\boldsymbol{\pi}_1, \dots, \boldsymbol{\pi}_m)$. In order to use a known closed-form solution of the NTK (Williams, 1996; Lee et al., 2019), we use a scaled error function $\sigma : \mathbb{R} \rightarrow (0, 1)$, resulting in the following decision function:

$$\begin{aligned} g_{m,n}(\mathbf{x}_i, \mathbf{w}_{m,n}) &= \sigma(\mathbf{w}_{m,n}^\top \mathbf{x}_i) \\ &:= \frac{1}{2} \operatorname{erf}(\alpha \mathbf{w}_{m,n}^\top \mathbf{x}_i) + \frac{1}{2}, \end{aligned} \quad (5)$$

where $\operatorname{erf}(p) = \frac{2}{\sqrt{\pi}} \int_0^p e^{-t^2} dt$ for any real scalar p . This scaled error function approximates commonly used sigmoid function. The scaling factor α is introduced by Frosst & Hinton (2017) to avoid too soft splitting. Figure 2 shows that when we increase α (from blue to red), the decision function becomes harder, and in the limit $\alpha \rightarrow \infty$ it coincides with the hard splitting used in typical decision trees.

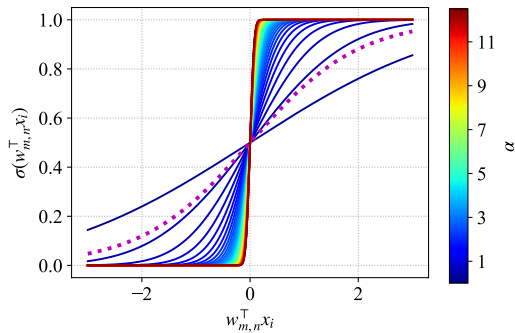


Figure 2: The scaled error function. We draw 50 lines with varying α by 0.25. A dotted magenta line shows a sigmoid function, which is close to a scaled error function with $\alpha \sim 0.5$.

When aggregating the output of multiple trees, we divide the sum of the tree outputs by the square root of the number of trees

$$f(\mathbf{x}_i, \mathbf{w}, \boldsymbol{\pi}) = \frac{1}{\sqrt{M}} \sum_{m=1}^M f_m(\mathbf{x}_i, \mathbf{w}_m, \boldsymbol{\pi}_m). \quad (6)$$

This $1/\sqrt{M}$ scaling is known to be essential in the existing NTK literature to use the weak law of the large numbers (Jacot et al., 2018). On top of Equation (6), we initialize model parameters $\mathbf{w}_{m,n}$ and $\boldsymbol{\pi}_{m,\ell}$ with zero-mean i.i.d. Gaussians with unit variances. We refer such a parameterization as *NTK initialization*.

In this paper, we consider a model such that all M trees have the same complete binary tree structure, a common setting for soft tree ensembles (Popov et al., 2020; Kontschieder et al., 2015; Hazimeh et al., 2020). The model output from a certain depth tree ensemble $f^{(d)}$ can be written alternatively using an incremental formula as

$$f^{(d)}(\mathbf{x}_i, \mathbf{w}, \boldsymbol{\pi}) = \frac{1}{\sqrt{M}} \sum_{m=1}^M \left(\sigma(\mathbf{w}_{m,t}^\top \mathbf{x}_i) f_m^{(d-1)}(\mathbf{x}_i, \mathbf{w}_m^{(l)}, \boldsymbol{\pi}_m^{(l)}) + (1 - \sigma(\mathbf{w}_{m,t}^\top \mathbf{x}_i)) f_m^{(d-1)}(\mathbf{x}_i, \mathbf{w}_m^{(r)}, \boldsymbol{\pi}_m^{(r)}) \right), \quad (7)$$

where indices (l) and (r) used with model parameters \mathbf{w}_m and $\boldsymbol{\pi}_m$ mean the parameters at the (l)eft subtree and the (r)ight subtree, respectively, and t used in $\mathbf{w}_{m,t}$ denotes the node at (t)op of the tree. For example, for trees of depth 3 as shown in Figure 1, $\mathbf{w}_m^{(l)} = (\mathbf{w}_{m,2}, \mathbf{w}_{m,4}, \mathbf{w}_{m,5})$, $\mathbf{w}_m^{(r)} = (\mathbf{w}_{m,3}, \mathbf{w}_{m,6}, \mathbf{w}_{m,7})$, and $\mathbf{w}_{m,t} = \mathbf{w}_{m,1}$.

4 Theoretical results

4.1 TNTK at initialization

We call the NTK (Equation (3)) induced by the soft tree ensembles introduced in Section 2.1 as the TNTK, and denote by $\hat{\Theta}_0^{(d)}(\mathbf{x}_i, \mathbf{x}_j)$ the TNTK at initialization induced by the ensemble of trees of depth d . In this section, we show the formula that the TNTK at initialization converges when considering the limit of infinite trees ($M \rightarrow \infty$).

Theorem 1. *Let $\mathbf{u} \in \mathbb{R}^{N_0 \times 1}$ be any column vector sampled from zero-mean i.i.d. Gaussians with unit variance. The TNTK for an ensemble of soft complete binary trees at tree depth d converges in probability to the following deterministic kernel as $M \rightarrow \infty$,*

$$\Theta^{(d)}(\mathbf{x}_i, \mathbf{x}_j) := \lim_{M \rightarrow \infty} \hat{\Theta}_0^{(d)}(\mathbf{x}_i, \mathbf{x}_j) = \underbrace{d(2^d)\Sigma(\mathbf{x}_i, \mathbf{x}_j)(\mathcal{T}(\mathbf{x}_i, \mathbf{x}_j))^{d-1}\dot{\mathcal{T}}(\mathbf{x}_i, \mathbf{x}_j)}_{\text{contribution from inner nodes}} + \underbrace{(2\mathcal{T}(\mathbf{x}_i, \mathbf{x}_j))^d}_{\text{contribution from leaves}}, \quad (8)$$

where $\Sigma(\mathbf{x}_i, \mathbf{x}_j) := \mathbf{x}_i^\top \mathbf{x}_j$, $\mathcal{T}(\mathbf{x}_i, \mathbf{x}_j) := \mathbb{E}[\sigma(\mathbf{u}^\top \mathbf{x}_i)\sigma(\mathbf{u}^\top \mathbf{x}_j)]$, $\dot{\mathcal{T}}(\mathbf{x}_i, \mathbf{x}_j) := \mathbb{E}[\dot{\sigma}(\mathbf{u}^\top \mathbf{x}_i)\dot{\sigma}(\mathbf{u}^\top \mathbf{x}_j)]$. Moreover, $\mathcal{T}(\mathbf{x}_i, \mathbf{x}_j)$ and $\dot{\mathcal{T}}(\mathbf{x}_i, \mathbf{x}_j)$ are analytically obtained in the closed-form as

$$\mathcal{T}(\mathbf{x}_i, \mathbf{x}_j) = \frac{1}{2\pi} \arcsin\left(\frac{\alpha^2 \Sigma(\mathbf{x}_i, \mathbf{x}_j)}{\sqrt{(\alpha^2 \Sigma(\mathbf{x}_i, \mathbf{x}_i) + 0.5)(\alpha^2 \Sigma(\mathbf{x}_j, \mathbf{x}_j) + 0.5)}}\right) + \frac{1}{4}, \quad (9)$$

$$\dot{\mathcal{T}}(\mathbf{x}_i, \mathbf{x}_j) = \frac{\alpha^2}{\pi} \frac{1}{\sqrt{(1 + 2\alpha^2 \Sigma(\mathbf{x}_i, \mathbf{x}_i))(1 + 2\alpha^2 \Sigma(\mathbf{x}_j, \mathbf{x}_j)) - 4\alpha^4 \Sigma(\mathbf{x}_i, \mathbf{x}_j)^2}}. \quad (10)$$

The dot used in $\dot{\sigma}(\mathbf{u}^\top \mathbf{x}_i)$ means the first derivative: $\frac{\alpha e^{-(\alpha \mathbf{u}^\top \mathbf{x}_i)^2}}{\sqrt{\pi}}$, and $\mathbb{E}[\cdot]$ means the expectation. The scalar π in Equation (9) and Equation (10) is the circular constant, and \mathbf{u} corresponds to $\mathbf{w}_{m,n}$ at an arbitrary internal node. The proof is given by induction. Due to the space limit, detailed proofs are given in the supplementary material.

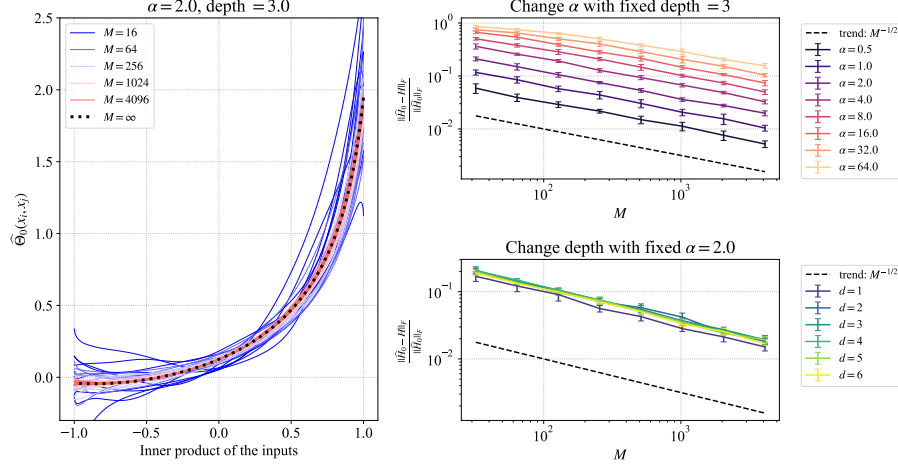


Figure 3: Left: An empirical demonstration of a convergence of the $\hat{\Theta}_0(x_i, x_j)$ to a fixed limit $\Theta(x_i, x_j)$. The $\hat{\Theta}_0^{(3)}(x_i, x_j)$ with $\alpha = 2.0$ is calculated and plotted 10 times with parameter re-initialization for each of the $m = 16, 64, 256, 1024$, and 4096 . Two simple inputs are considered: $x_i = \{1, 0\}$ and $x_j = \{\cos(\beta), \sin(\beta)\}$, where $\beta = [0, \pi]$. Right: Parameter dependency of the convergence. The vertical axis corresponds to the averaged error between the \hat{H}_0 and the $H := \lim_{M \rightarrow \infty} \hat{H}_0$ for 50 random unit vectors of length $N_0 = 5$. The dashed lines are plotted only for showing the slope, and the intercept does not matter. The error-bars show the standard deviations of 10 executions.

The Figure 3 visualizes Theorem 1. The TNTK induced by sufficiently many soft trees converges to the right-hand side of Equation (8). The limiting TNTK is similar to the kernel induced by an ensemble of several hundred trees, which is a typical order of the number of trees in practical applications¹.

Remarks. The MLP and tree ensemble models are apparently different. However, we derived our proof by pointing out the similarities between the soft tree ensembles and MLP. On the one hand, by using the same symbols used in soft trees to make it easier to see the correspondences, we consider a two-layer perceptron as $\frac{1}{\sqrt{M}} \sum_{m=1}^M a_m \sigma(w_m^\top x_i)$, where we use M as the number of the hidden layer nodes, σ as a nonlinear activation function of the MLP, and $w = (w_1, \dots, w_m) \in \mathbb{R}^{N_0 \times M}$ and $a = (a_1, \dots, a_m) \in \mathbb{R}^{1 \times M}$ as parameters at the first and second layers initialized by zero-mean Gaussians with unit variances. On the other hand, changing the notation back to that for tree ensembles as defined in Section 2.1, an output of a soft tree ensemble of depth 1 is $\frac{1}{\sqrt{M}} \sum_{m=1}^M \sigma(w_{m,1}^\top x_i) \pi_{m,1} + (1 - \sigma(w_{m,1}^\top x_i)) \pi_{m,2}$. With a small deformation, we obtain $\frac{1}{\sqrt{M}} \sum_{m=1}^M ((\pi_{m,1} - \pi_{m,2}) \sigma(w_{m,1}^\top x_i) + \pi_{m,2})$. If we ignore the offset term $+\pi_{m,2}$ at the end of the right-hand side, compared to the MLP, the tree splitting operation and the tree leaves correspond to the processing of the first layer in the MLP and the second layer in the MLP, respectively. In addition, one can also find the correspondence between the number of trees and the number of hidden layer nodes in the MLP. This correspondence is one of our motivations for considering infinite tree ensembles using the NTK theory, which leads to our theoretical result (Theorem 1) using results of the MLP with infinite width (Jacot et al., 2018).

4.1.1 Influence of the oblivious tree structure

An oblivious tree is a practical tree model architecture, where the rules across decision tree splitting are shared for the same depth as illustrated in Figure 4. Since the number of the splitting decision calculation can be reduced from $\mathcal{O}(2^d)$ to $\mathcal{O}(d)$, the oblivious tree structure is used in various open-source libraries such as CatBoost (Prokhorenkova et al., 2018) and NODE (Popov et al., 2020).

¹For example, Popov et al. (2020) uses 2048 trees.

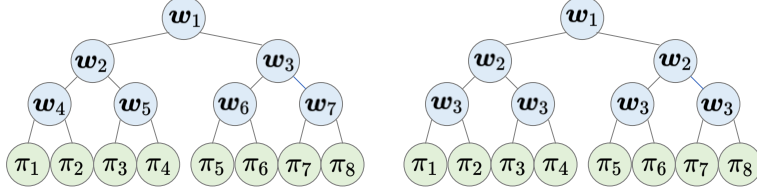


Figure 4: Left: Normal Tree, Right: Oblivious Tree. The rules for splitting in the same depth are shared across the same depth in the oblivious tree, while $\pi_{m,\ell}$ on leaves can be different.

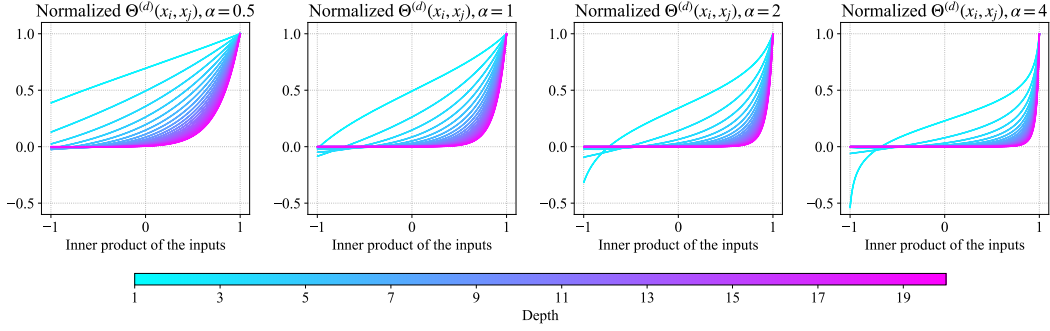


Figure 5: Depth dependencies of $\Theta^{(d)}(\mathbf{x}_i, \mathbf{x}_j)$. The vertical axes are normalized so that the value is 1 when the inner product of the inputs is 1. Input vector size is normalized to be one. We illustrate four cases with $\alpha = 0.5, 1, 2$, and 4 , and draw 20 lines with varying the depth by 1 in each plot.

Using an incremental formula, the output from the oblivious tree ensembles can be written as follows:

$$f^{(d)}(\mathbf{x}_i, \mathbf{w}, \boldsymbol{\pi}) = \frac{1}{\sqrt{M}} \sum_{m=1}^M \left(\sigma(\mathbf{w}_{m,t}^\top \mathbf{x}_i) f_m^{(d-1)}(\mathbf{x}_i, \mathbf{w}_m^{(s)}, \boldsymbol{\pi}_m^{(l)}) + (1 - \sigma(\mathbf{w}_{m,t}^\top \mathbf{x}_i)) f_m^{(d-1)}(\mathbf{x}_i, \mathbf{w}_m^{(s)}, \boldsymbol{\pi}_m^{(r)}) \right), \quad (11)$$

where (s) of $\mathbf{w}_m^{(s)}$ means (s) hared parameters at subtrees. Even with parameter sharing at the splitting nodes, since the leaf parameters $\boldsymbol{\pi}$ are not shared, the left and right subtree's outputs are independent. Therefore, we find that the oblivious tree structure does not change the resulting TNTK from the non-oblivious one.

Theorem 2. *The TNTK obtained from the complete binary oblivious tree ensemble and the TNTK with the complete binary non-oblivious tree ensemble converge to the same kernel in probability in the limit of infinite trees ($M \rightarrow \infty$) as long as the tree depth is the same.*

Note that the leaf values $\boldsymbol{\pi}$ do not have to be same for oblivious and non-oblivious trees. The complete proof is in the supplementary material. The reason for the good empirical performance despite weakening the expressive power by the parameter sharing is non-trivial. This theorem supports the recent success of tree ensemble models with the oblivious tree structure such as CatBoost (Prokhorenkova et al., 2018) and NODE (Popov et al., 2020).

4.1.2 Degeneracy caused by deep trees

As the depth increases, $\mathcal{T}(\mathbf{x}_i, \mathbf{x}_j)$ defined in Equation (9), which consists of the arcsine function, is multiplied multiple times to calculate the limiting TNTK in Equation (8). Therefore, when we increase the depth too much, the resulting TNTK exhibits degeneracy: its output values are almost the same with each other even though the input's inner products are different. Figure 5 shows such a degeneracy behavior. In terms of kernel regression, models using a kernel that gives almost the same inner product to all data except for those that are quite close to each other are expected to have poor generalization performance. Such behavior is observed in our numerical experiments (Section 5). Huang et al. (2020) showed that typical deep neural networks also exhibit such degeneracy when the

number of layers increases. Our observation is substantially similar to their observation. In practical applications, one does not usually use too deep soft or hard decision trees. This degeneracy of the TNTK supports the poor performance when the tree is too deep (Luo et al., 2021).

4.1.3 Positive definiteness of the limiting TNTK

Jacot et al. (2018) have shown that the conditions $\|x_i\|_2 = 1$ for all $i \in [N]$ and $x_i \neq x_j$ ($i \neq j$) are necessary for the positive definiteness of the NTK induced by the MLP for an input set. This assumption is commonly used in the study of NTK (Lee et al., 2019). Under the same condition, the TNTK induced by infinite trees is also positive definite.

Proposition 1. *For infinitely many soft trees with any depth and the NTK initialization, the limiting TNTK is positive definite if $\|x_i\|_2 = 1$ for all $i \in [N]$ and $x_i \neq x_j$ ($i \neq j$).*

The proof based on Jacot et al. (2018) is in the supplementary material.

Remarks. Since the loss surface of the large model is expected to be highly non-convex, understanding of the empirical good trainability of the overparameterized models is still an open problem (Dauphin et al., 2014). If the limiting TNTK is constant during training, the positive definiteness of the limiting TNTK at initialization indicates that training of the infinite trees with a gradient method can converge to the global minimum, which supports the empirical success of overparameterized models. We prove that the limiting TNTK is constant in the next section.

4.2 Change of the TNTK during training

We prove that the TNTK hardly changes from its initial value during training when considering an ensemble of infinite trees if α in Equation (5) is finite.

Theorem 3. *Let λ_{\min} and λ_{\max} be the minimum and maximum eigenvalues of the limiting TNTK. Assume that the limiting TNTK is positive definite for input sets. For soft tree ensemble models with the NTK initialization and a positive finite scaling factor α trained under gradient flow with a learning rate $\eta < 2/(\lambda_{\min} + \lambda_{\max})$, we have with high probability*

$$\sup \left| \hat{\Theta}_{\tau}^{(d)}(x_i, x_j) - \hat{\Theta}_0^{(d)}(x_i, x_j) \right| = \mathcal{O} \left(\frac{1}{\sqrt{M}} \right). \quad (12)$$

Note that this theorem also holds for the ensemble of oblivious trees. The complete proof is in the supplementary material.

Remarks. If we consider the case where the number M of trees is infinite, the TNTK does not change during training. It implies that training of the infinite trees with the gradient method can converge to a global minimum, as discussed in Section 4.2. In the limit of infinitely large α as in a hard decision tree splitting (Figure 2), it should be noted that this theorem does not hold because of the lack of local Lipschitzness, which is the fundamental property for this proof (Lee et al., 2019). Therefore, the change in the TNTK during training is no longer necessarily asymptotic to zero even if the number of trees is infinite. Even if we get some useful suggestions for soft tree ensembles, understanding the hard decision tree’s behavior using the TNTK is not straightforward.

5 Numerical Experiments

We present our experimental results on 90 classification tasks in the UCI database (Dua & Graff, 2017), with less than 5000 data points as in Arora et al. (2020). We performed kernel regression using the limiting TNTK defined in Equation (8) with varying parameters, the tree depth (d) and the scaling (α) of the decision function. Assuming an infinite ensemble of soft trees, the limiting TNTK does not change during training. Hence, predictions from that model are equivalent to kernel regression using the limiting TNTK (Jacot et al., 2018). For considering the ridge-less situation, regularization strength is set to be 1.0×10^{-8} , a very small constant. For a comparison, performances of the kernel regression with the MLP-induced NTK (Jacot et al., 2018) and the RBF kernel are also reported. For the MLP-induced NTK, we assume the MLP activation function as ReLU. We follow the procedures of Arora et al. (2020) and Fernández-Delgado et al. (2014): We report 4-fold cross-validation performance with random data splitting. To tune the parameter, all available training

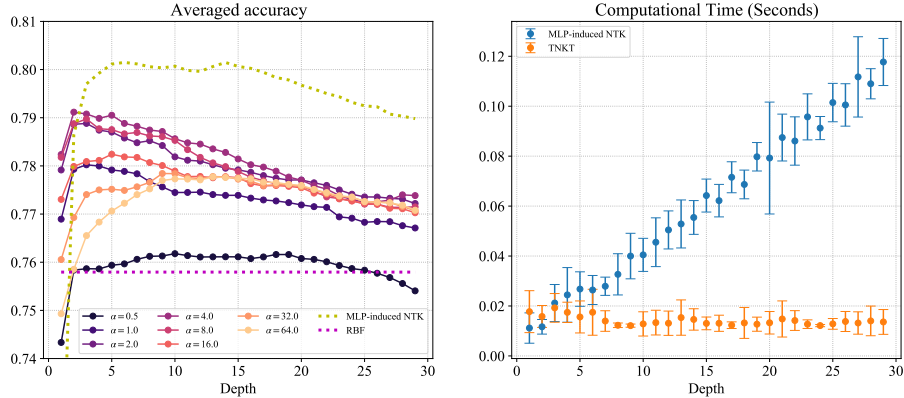


Figure 6: Left: Averaged accuracy over 90 datasets. The performances of the kernel regression with the MLP-induced NTK and the RBF kernel are shown for comparison. Since the depth is not a hyperparameter of the RBF kernel, performance is shown by a horizontal line. The statistical significance is also assessed in the supplementary material. Right: Running time for kernel computation. The input dataset has 300 samples with 10 features. Feature values are generated by zero-mean i.i.d Gaussian with unit variance. The error-bars show the standard deviations of 10 executions.

	TNTK									RBF
α	0.5	1.0	2.0	4.0	8.0	16.0	32.0	64.0		
Win rate (%)	13.6	18.8	22.2	28.6	32.5	31.6	34.9	27.2		11.8

Table 1: Performance win rate against MLP-induced NTK. We tune the depth among $d = 1$ to 29 for the dataset-wise comparison for both the TNTK and the MLP-induced NTK. For RBF kernel, 30 different hyperparameters are tried. Detailed results are in the supplementary material.

samples are randomly split into one training and one validation set, while imposing that each class has the same number of training and validation samples. Then the parameter with the best validation accuracy is selected. Other details are in the supplementary material.

The left panel of Figure 6 shows the averaged performance as a function of the depth. Although the TNTK results with proper parameters tend to be better than those obtained with the RBF kernel, they are often inferior to the MLP-induced NTK. The results support the good performance of the MLP-induced NTK (Arora et al., 2020). It should be noted that when we look at each dataset one by one, the TNTK is superior to the MLP-induced NTK for more than 30% of the dataset, as shown in Table 1. This is a case where the characteristics of data and the inductive bias of the model fit well together. In addition, although the MLP-induced NTK has a computational cost linear to the depth of the model because of the recursive computation (Jacot et al., 2018), the TNTK’s computational cost does not depend on the depth, as shown in Equation (8) and the right panel of Figure 6. Even if the MLP-induced NTK is better in prediction accuracy, the TNTK may be used in practical cases as a trade-off for computational complexity. Arora et al. (2019a) proposes the use of the NTK for a neural architecture search (Elsken et al., 2019; Chen et al., 2021). In such applications, the fast computation of the kernel in various architectures can be a benefit. We leave extensions of this idea to tree models as future work.

When we increase the tree depth, we observe an improvement in performance at the beginning. After that, the performance gradually decreases. This behavior is consistent with the performance deterioration due to degeneracy (Section 4.1.2), similar to that reported for neural networks without skip-connection (Huang et al., 2020) shown with the dotted yellow line. The performance improvement by adjusting α in the decision function (Frosst & Hinton, 2017; Popov et al., 2020; Arik & Pfister, 2019) is also observed. As long as we do not take the value too extreme, it is almost always better than the sigmoid-like function ($\alpha = 0.5$, as shown in Figure 2).

6 Conclusions

In this paper, we have introduced and studied the *Tree Neural Tangent Kernel* (TNTK) by considering the ensemble of infinitely many soft trees. The TNTK provides new insights into the behavior of the infinite ensemble of soft trees, such as the effect of the oblivious tree structure and the degeneracy of the TNTK induced by the deepening of the trees. In numerical experiments, we have observed the degeneracy phenomena induced by the deepening of the soft tree model, which is suggested by our theoretical results. To date, the NTK theory has been mostly applied to neural networks, and our study is the first to apply it to the tree model. Therefore our study will be a milestone of further development of the NTK theory. We believe that the TNTK’s theoretical analysis will not have a negative impact on society as our work does not directly lead to harmful applications.

References

- Sina Alemohammad, Zichao Wang, Randall Balestriero, and Richard Baraniuk. The Recurrent Neural Tangent Kernel. In *International Conference on Learning Representations*, 2021.
- Sercan Ömer Arik and Tomas Pfister. TabNet: Attentive Interpretable Tabular Learning. *CoRR*, abs/1908.07442, 2019.
- Sanjeev Arora, Simon S Du, Wei Hu, Zhiyuan Li, Russ R Salakhutdinov, and Ruosong Wang. On Exact Computation with an Infinitely Wide Neural Net. In *Advances in Neural Information Processing Systems*, volume 32, 2019a.
- Sanjeev Arora, Simon S Du, Wei Hu, Zhiyuan Li, Russ R Salakhutdinov, and Ruosong Wang. On Exact Computation with an Infinitely Wide Neural Net. In *Advances in Neural Information Processing Systems*. 2019b.
- Sanjeev Arora, Simon S. Du, Zhiyuan Li, Ruslan Salakhutdinov, Ruosong Wang, and Dingli Yu. Harnessing the Power of Infinitely Wide Deep Nets on Small-data Tasks. In *International Conference on Learning Representations*, 2020.
- Mikhail Belkin, Daniel Hsu, Siyuan Ma, and Soumik Mandal. Reconciling modern machine-learning practice and the classical bias–variance trade-off. *Proceedings of the National Academy of Sciences*, 116(32), 2019.
- Leo Breiman. Random Forests. In *Machine Learning*, 2001.
- Leo Breiman, Jerome Friedman, Charles J. Stone, and R.A. Olshen. *Classification and Regression Trees*. Chapman and Hall/CRC, 1984.
- Wuyang Chen, Xinyu Gong, and Zhangyang Wang. Neural Architecture Search on ImageNet in Four GPU Hours: A Theoretically Inspired Perspective. In *International Conference on Learning Representations*, 2021.
- Yann N Dauphin, Razvan Pascanu, Caglar Gulcehre, Kyunghyun Cho, Surya Ganguli, and Yoshua Bengio. Identifying and attacking the saddle point problem in high-dimensional non-convex optimization. In *Advances in Neural Information Processing Systems*, volume 27, 2014.
- Simon S Du, Kangcheng Hou, Russ R Salakhutdinov, Barnabas Poczos, Ruosong Wang, and Keyulu Xu. Graph Neural Tangent Kernel: Fusing Graph Neural Networks with Graph Kernels. In *Advances in Neural Information Processing Systems*, volume 32, 2019.
- Dheeru Dua and Casey Graff. UCI Machine Learning Repository, 2017. URL <http://archive.ics.uci.edu/ml>.
- Thomas Elsken, Jan Hendrik Metzen, and Frank Hutter. Neural Architecture Search: A Survey. *Journal of Machine Learning Research*, 20(55):1–21, 2019.
- Manuel Fernández-Delgado, Eva Cernadas, Senén Barro, and Dinani Amorim. Do we Need Hundreds of Classifiers to Solve Real World Classification Problems? *Journal of Machine Learning Research*, 15, 2014.

- Nicholas Frosst and Geoffrey E. Hinton. Distilling a Neural Network Into a Soft Decision Tree. *CoRR*, 2017.
- Hussein Hazimeh, Natalia Ponomareva, Petros Mol, Zhenyu Tan, and Rahul Mazumder. The Tree Ensemble Layer: Differentiability meets Conditional Computation. In *Proceedings of the 37th International Conference on Machine Learning*, volume 119, 2020.
- Kaixuan Huang, Yuqing Wang, Molei Tao, and Tuo Zhao. Why Do Deep Residual Networks Generalize Better than Deep Feedforward Networks? — A Neural Tangent Kernel Perspective. In *Advances in Neural Information Processing Systems*, volume 33, 2020.
- Laurent Hyafil and Ronald L. Rivest. Constructing optimal binary decision trees is NP-complete. *Information Processing Letters*, 5(1), 1976.
- Arthur Jacot, Franck Gabriel, and Clement Hongler. Neural Tangent Kernel: Convergence and Generalization in Neural Networks. In *Advances in Neural Information Processing Systems 31*. 2018.
- M.I. Jordan and R.A. Jacobs. Hierarchical mixtures of experts and the EM algorithm. In *Proceedings of 1993 International Conference on Neural Networks*, volume 2, 1993.
- Ajaykrishna Karthikeyan, Naman Jain, Nagarajan Natarajan, and Prateek Jain. Learning Accurate Decision Trees with Bandit Feedback via Quantized Gradient Descent. *CoRR*, 2021.
- Guolin Ke, Zhenhui Xu, Jia Zhang, Jiang Bian, and Tie-Yan Liu. DeepGBM: A Deep Learning Framework Distilled by GBDT for Online Prediction Tasks. In *Proceedings of the 25th ACM SIGKDD International Conference on Knowledge Discovery & Data Mining*, 2019.
- Peter Kontschieder, Madalina Fiterau, Antonio Criminisi, and Samuel Rota Bulò. Deep Neural Decision Forests. In *2015 IEEE International Conference on Computer Vision*, 2015.
- Jaehoon Lee, Lechao Xiao, Samuel Schoenholz, Yasaman Bahri, Roman Novak, Jascha Sohl-Dickstein, and Jeffrey Pennington. Wide Neural Networks of Any Depth Evolve as Linear Models Under Gradient Descent. In *Advances in Neural Information Processing Systems*, volume 32, 2019.
- Dmitry Lepikhin, HyoukJoong Lee, Yuanzhong Xu, Dehao Chen, Orhan Firat, Yanping Huang, Maxim Krikun, Noam Shazeer, and Zhifeng Chen. GShard: Scaling Giant Models with Conditional Computation and Automatic Sharding. In *International Conference on Learning Representations*, 2021.
- Zhiyuan Li, Ruosong Wang, Dingli Yu, Simon S. Du, Wei Hu, Ruslan Salakhutdinov, and Sanjeev Arora. Enhanced Convolutional Neural Tangent Kernels. *CoRR*, abs/1911.00809, 2019.
- Haoran Luo, Fan Cheng, Heng Yu, and Yuqi Yi. SDTR: Soft Decision Tree Regressor for Tabular Data. *IEEE Access*, 9, 2021.
- Sergei Popov, Stanislav Morozov, and Artem Babenko. Neural Oblivious Decision Ensembles for Deep Learning on Tabular Data. In *International Conference on Learning Representations*, 2020.
- Liudmila Prokhorenkova, Gleb Gusev, Aleksandr Vorobev, Anna Veronika Dorogush, and Andrey Gulin. CatBoost: unbiased boosting with categorical features. In *Advances in Neural Information Processing Systems*, volume 31, 2018.
- J. R. Quinlan. Induction of Decision Trees. *Machine Learning*, 1(1), 1986.
- Noam Shazeer, Azalia Mirhoseini, Krzysztof Maziarczyk, Andy Davis, Quoc V. Le, Geoffrey E. Hinton, and Jeff Dean. Outrageously Large Neural Networks: The Sparsely-Gated Mixture-of-Experts Layer. In *International Conference on Learning Representations*, 2017.
- Ryutaro Tanno, Kai Arulkumaran, Daniel Alexander, Antonio Criminisi, and Aditya Nori. Adaptive Neural Trees. In *Proceedings of the 36th International Conference on Machine Learning*, volume 97, 2019.

Alvin Wan, Lisa Dunlap, Daniel Ho, Jihan Yin, Scott Lee, Suzanne Petryk, Sarah Adel Bargal, and Joseph E. Gonzalez. NBDT: Neural-Backed Decision Tree. In *International Conference on Learning Representations*, 2021.

Christopher K. I. Williams. Computing with Infinite Networks. In *Advances in Neural Information Processing Systems*, 1996.

A Proof of Theorem 1

Proof. We prove the theorem by induction. When $d = 1$,

$$f^{(1)}(\mathbf{x}_i, \mathbf{w}, \boldsymbol{\pi}) = \frac{1}{\sqrt{M}} \sum_{m=1}^M \left(\sigma(\mathbf{w}_{m,1}^\top \mathbf{x}_i) \pi_{m,1} + (1 - \sigma(\mathbf{w}_{m,1}^\top \mathbf{x}_i)) \pi_{m,2} \right). \quad (\text{A.1})$$

Derivatives are

$$\frac{\partial f^{(1)}(\mathbf{x}_i, \mathbf{w}, \boldsymbol{\pi})}{\partial \mathbf{w}_{m,1}} = \frac{1}{\sqrt{M}} (\pi_{m,1} - \pi_{m,2}) \mathbf{x}_i \dot{\sigma}(\mathbf{w}_{m,1}^\top \mathbf{x}_i), \quad (\text{A.2})$$

$$\frac{\partial f^{(1)}(\mathbf{x}_i, \mathbf{w}, \boldsymbol{\pi})}{\partial \pi_{m,1}} = \frac{1}{\sqrt{M}} \sigma(\mathbf{w}_{m,1}^\top \mathbf{x}_i), \quad (\text{A.3})$$

$$\frac{\partial f^{(1)}(\mathbf{x}_i, \mathbf{w}, \boldsymbol{\pi})}{\partial \pi_{m,2}} = -\frac{1}{\sqrt{M}} (1 - \sigma(\mathbf{w}_{m,1}^\top \mathbf{x}_i)), \quad (\text{A.4})$$

Therefore, since there is only one internal node per a single tree, from the definition of the NTK, the TNTK is obtained as

$$\begin{aligned} \hat{\Theta}^{(1)}(\mathbf{x}_i, \mathbf{x}_j) &= \sum_{m=1}^M \left(\left\langle \frac{\partial f(\mathbf{x}_i, \mathbf{w}, \boldsymbol{\pi})}{\partial \mathbf{w}_{m,1}}, \frac{\partial f(\mathbf{x}_j, \mathbf{w}, \boldsymbol{\pi})}{\partial \mathbf{w}_{m,1}} \right\rangle \right. \\ &\quad \left. + \left\langle \frac{\partial f(\mathbf{x}_i, \mathbf{w}, \boldsymbol{\pi})}{\partial \pi_{m,1}}, \frac{\partial f(\mathbf{x}_j, \mathbf{w}, \boldsymbol{\pi})}{\partial \pi_{m,1}} \right\rangle + \left\langle \frac{\partial f(\mathbf{x}_i, \mathbf{w}, \boldsymbol{\pi})}{\partial \pi_{m,2}}, \frac{\partial f(\mathbf{x}_j, \mathbf{w}, \boldsymbol{\pi})}{\partial \pi_{m,2}} \right\rangle \right) \\ &= \frac{1}{M} \sum_{m=1}^M \left((\pi_{m,1} - \pi_{m,2})^2 \mathbf{x}_i^\top \mathbf{x}_j \dot{\sigma}(\mathbf{w}_{m,1}^\top \mathbf{x}_i) \dot{\sigma}(\mathbf{w}_{m,1}^\top \mathbf{x}_j) + 2\sigma(\mathbf{w}_{m,1}^\top \mathbf{x}_i) \sigma(\mathbf{w}_{m,1}^\top \mathbf{x}_j) \right). \end{aligned} \quad (\text{A.5})$$

Since we are considering the infinite number of trees ($M \rightarrow \infty$), the average in Equation (A.5) can be replaced by the expected value by applying the law of the large numbers:

$$\begin{aligned} \Theta^{(1)}(\mathbf{x}_i, \mathbf{x}_j) &= \mathbb{E}_m \left[\left((\pi_{m,1} - \pi_{m,2})^2 \mathbf{x}_i^\top \mathbf{x}_j \dot{\sigma}(\mathbf{w}_{m,1}^\top \mathbf{x}_i) \dot{\sigma}(\mathbf{w}_{m,1}^\top \mathbf{x}_j) \right. \right. \\ &\quad \left. \left. + 2\sigma(\mathbf{w}_{m,1}^\top \mathbf{x}_i) \sigma(\mathbf{w}_{m,1}^\top \mathbf{x}_j) \right) \right] \\ &= 2(\Sigma(\mathbf{x}_i, \mathbf{x}_j) \dot{\mathcal{T}}(\mathbf{x}_i, \mathbf{x}_j) + \mathcal{T}(\mathbf{x}_i, \mathbf{x}_j)), \end{aligned} \quad (\text{A.6})$$

which is consistent with Equation (8). Here, $\mathbb{E}_m \left[(\pi_{m,1} - \pi_{m,2})^2 \right] = 2$ because the variance of $\pi_{m,\ell}$ is 1.0, and $\mathbf{w}_{m,1}$ corresponds to \mathbf{u} in Theorem 1.

For $d > 1$, we divide the TNTK into four components:

$$\Theta^{(d)}(\mathbf{x}_i, \mathbf{x}_j) = \Theta^{(d),(t)}(\mathbf{x}_i, \mathbf{x}_j) + \Theta^{(d),(l)}(\mathbf{x}_i, \mathbf{x}_j) + \Theta^{(d),(r)}(\mathbf{x}_i, \mathbf{x}_j) + \Theta^{(d),(b)}(\mathbf{x}_i, \mathbf{x}_j),$$

where the indices (t) , (l) and (r) mean the parameters of the (t)op of the tree, (l)eft subtree, and (r)ight subtree, respectively. The index (b) implies the (b)ottom of the tree: tree leaves. With Equation (A.6),

we have

$$\Theta^{(1),(t)}(\mathbf{x}_i, \mathbf{x}_j) = 2\Sigma(\mathbf{x}_i, \mathbf{x}_j)\dot{\mathcal{T}}(\mathbf{x}_i, \mathbf{x}_j), \quad (\text{A.7})$$

$$\Theta^{(1),(l)}(\mathbf{x}_i, \mathbf{x}_j) = 0, \quad (\text{A.8})$$

$$\Theta^{(1),(r)}(\mathbf{x}_i, \mathbf{x}_j) = 0, \quad (\text{A.9})$$

$$\Theta^{(1),(b)}(\mathbf{x}_i, \mathbf{x}_j) = 2\mathcal{T}(\mathbf{x}_i, \mathbf{x}_j). \quad (\text{A.10})$$

For each component, we show the following lemmas:

Lemma 1.

$$\Theta^{(d+1),(t)}(\mathbf{x}_i, \mathbf{x}_j) = 2\mathcal{T}(\mathbf{x}_i, \mathbf{x}_j)\Theta^{(d),(t)}(\mathbf{x}_i, \mathbf{x}_j) \quad (\text{A.11})$$

Lemma 2.

$$\begin{aligned} & \Theta^{(d+1),(l)}(\mathbf{x}_i, \mathbf{x}_j) + \Theta^{(d+1),(r)}(\mathbf{x}_i, \mathbf{x}_j) \\ &= 2\mathcal{T}(\mathbf{x}_i, \mathbf{x}_j)(\Theta^{(d),(t)}(\mathbf{x}_i, \mathbf{x}_j) + \Theta^{(d),(l)}(\mathbf{x}_i, \mathbf{x}_j) + \Theta^{(d),(r)}(\mathbf{x}_i, \mathbf{x}_j)) \end{aligned} \quad (\text{A.12})$$

Lemma 3.

$$\Theta^{(d+1),(b)}(\mathbf{x}_i, \mathbf{x}_j) = 2\mathcal{T}(\mathbf{x}_i, \mathbf{x}_j)\Theta^{(d),(b)}(\mathbf{x}_i, \mathbf{x}_j) \quad (\text{A.13})$$

Combining them, we can derive Equation (8). \square

A.1 Proof of Lemma 1

Proof. An incremental formula for the model output with a certain depth tree ensemble is

$$\begin{aligned} f^{(d)}(\mathbf{x}_i, \mathbf{w}, \boldsymbol{\pi}) &= \frac{1}{\sqrt{M}} \sum_{m=1}^M \left(\sigma(\mathbf{w}_{m,t}^\top \mathbf{x}_i) f_m^{(d-1)}(\mathbf{x}_i, \mathbf{w}_m^{(l)}, \boldsymbol{\pi}_m^{(l)}) \right. \\ &\quad \left. + (1 - \sigma(\mathbf{w}_{m,t}^\top \mathbf{x}_i)) f_m^{(d-1)}(\mathbf{x}_i, \mathbf{w}_m^{(r)}, \boldsymbol{\pi}_m^{(r)}) \right), \end{aligned} \quad (\text{A.14})$$

where t used in $\mathbf{w}_{m,t}$ implies the node at the top of the tree. With Equation (A.14),

$$\frac{\partial f^{(d+1)}(\mathbf{x}_i, \mathbf{w}, \boldsymbol{\pi})}{\partial \mathbf{w}_{m,t}} = \mathbf{x}_i \dot{\sigma}(\mathbf{w}_{m,t}^\top \mathbf{x}_i) \left(f_m^{(d)}(\mathbf{x}_i, \mathbf{w}_m^{(l)}, \boldsymbol{\pi}_m^{(l)}) - f_m^{(d)}(\mathbf{x}_i, \mathbf{w}_m^{(r)}, \boldsymbol{\pi}_m^{(r)}) \right), \quad (\text{A.15})$$

$$\begin{aligned} \hat{\Theta}^{(d+1),(t)}(\mathbf{x}_i, \mathbf{x}_j) &= \frac{1}{M} \sum_{m=1}^M \mathbf{x}_i^\top \mathbf{x}_j \dot{\sigma}(\mathbf{w}_{m,t}^\top \mathbf{x}_i) \dot{\sigma}(\mathbf{w}_{m,t}^\top \mathbf{x}_j) \left(f_m^{(d)}(\mathbf{x}_i, \mathbf{w}_m^{(l)}, \boldsymbol{\pi}_m^{(l)}) f_m^{(d)}(\mathbf{x}_j, \mathbf{w}_m^{(l)}, \boldsymbol{\pi}_m^{(l)}) \right. \\ &\quad - f_m^{(d)}(\mathbf{x}_i, \mathbf{w}_m^{(l)}, \boldsymbol{\pi}_m^{(l)}) f_m^{(d)}(\mathbf{x}_j, \mathbf{w}_m^{(r)}, \boldsymbol{\pi}_m^{(r)}) \\ &\quad - f_m^{(d)}(\mathbf{x}_i, \mathbf{w}_m^{(r)}, \boldsymbol{\pi}_m^{(r)}) f_m^{(d)}(\mathbf{x}_j, \mathbf{w}_m^{(l)}, \boldsymbol{\pi}_m^{(l)}) \\ &\quad \left. + f_m^{(d)}(\mathbf{x}_i, \mathbf{w}_m^{(r)}, \boldsymbol{\pi}_m^{(r)}) f_m^{(d)}(\mathbf{x}_j, \mathbf{w}_m^{(r)}, \boldsymbol{\pi}_m^{(r)}) \right), \end{aligned} \quad (\text{A.16})$$

Since $f_m^{(d)}(\mathbf{x}_i, \mathbf{w}_m^{(r)}, \boldsymbol{\pi}_m^{(r)})$ and $f_m^{(d)}(\mathbf{x}_j, \mathbf{w}_m^{(l)}, \boldsymbol{\pi}_m^{(l)})$ are independent to each other and have zero-mean Gaussian distribution because of the initialization of $\boldsymbol{\pi}_m$ with zero-mean i.i.d Gaussians², $\mathbb{E} \left[f_m^{(d)}(\mathbf{x}_i, \mathbf{w}_m^{(l)}, \boldsymbol{\pi}_m^{(l)}) f_m^{(d)}(\mathbf{x}_j, \mathbf{w}_m^{(r)}, \boldsymbol{\pi}_m^{(r)}) \right]$ and $\mathbb{E} \left[f_m^{(d)}(\mathbf{x}_i, \mathbf{w}_m^{(r)}, \boldsymbol{\pi}_m^{(r)}) f_m^{(d)}(\mathbf{x}_j, \mathbf{w}_m^{(l)}, \boldsymbol{\pi}_m^{(l)}) \right]$ are zero. Therefore, considering the infinite number of trees ($M \rightarrow \infty$),

$$\begin{aligned} \Theta^{(d+1),(t)}(\mathbf{x}_i, \mathbf{x}_j) &= \mathbf{x}_i^\top \mathbf{x}_j \dot{\mathcal{T}}(\mathbf{x}_i, \mathbf{x}_j) \mathbb{E}_m \left[f_m^{(d)}(\mathbf{x}_i, \mathbf{w}_m^{(l)}, \boldsymbol{\pi}_m^{(l)}) f_m^{(d)}(\mathbf{x}_j, \mathbf{w}_m^{(l)}, \boldsymbol{\pi}_m^{(l)}) \right. \\ &\quad \left. + f_m^{(d)}(\mathbf{x}_i, \mathbf{w}_m^{(r)}, \boldsymbol{\pi}_m^{(r)}) f_m^{(d)}(\mathbf{x}_j, \mathbf{w}_m^{(r)}, \boldsymbol{\pi}_m^{(r)}) \right] \end{aligned} \quad (\text{A.17})$$

²This holds due to the fact that model output is a weighted average of $\pi_{m,\ell}$.

From Equation (A.17), what we need to prove is $\mathbb{E}_m \left[f_m^{(d)}(\mathbf{x}_i, \mathbf{w}_m, \boldsymbol{\pi}_m) f_m^{(d)}(\mathbf{x}_j, \mathbf{w}_m, \boldsymbol{\pi}_m) \right] = (2\mathcal{T}(\mathbf{x}_i, \mathbf{x}_j))^d$. We prove it by induction. In the base case with $d = 1$,

$$\begin{aligned}
& \mathbb{E}_m \left[f_m^{(1)}(\mathbf{x}_i, \mathbf{w}_m, \boldsymbol{\pi}_m) f_m^{(1)}(\mathbf{x}_j, \mathbf{w}_m, \boldsymbol{\pi}_m) \right] \\
&= \mathbb{E}_m \left[\left(\sigma(\mathbf{w}_{m,1}^\top \mathbf{x}_i) \pi_{m,1} + (1 - \sigma(\mathbf{w}_{m,1}^\top \mathbf{x}_i)) \pi_{m,2} \right) \left(\sigma(\mathbf{w}_{m,1}^\top \mathbf{x}_j) \pi_{m,1} + (1 - \sigma(\mathbf{w}_{m,1}^\top \mathbf{x}_j)) \pi_{m,2} \right) \right] \\
&= \mathbb{E}_m \left[\underbrace{(\pi_{m,1} - \pi_{m,2})^2}_{\rightarrow 2} \sigma(\mathbf{w}_{m,1}^\top \mathbf{x}_i) \sigma(\mathbf{w}_{m,1}^\top \mathbf{x}_j) \right. \\
&\quad \left. + \underbrace{\pi_{m,1} \pi_{m,2}}_{\rightarrow 0} (\sigma(\mathbf{w}_{m,1}^\top \mathbf{x}_i) + \sigma(\mathbf{w}_{m,1}^\top \mathbf{x}_j)) - \pi_{m,2}^2 \underbrace{(\sigma(\mathbf{w}_{m,1}^\top \mathbf{x}_i) + \sigma(\mathbf{w}_{m,1}^\top \mathbf{x}_j) - 1)}_{\rightarrow 0} \right] \\
&= 2\mathcal{T}(\mathbf{x}_i, \mathbf{x}_j), \tag{A.18}
\end{aligned}$$

where we use the property

$$\mathbb{E}[\sigma(v)] = 0.5 \tag{A.19}$$

for any v generated from a zero-mean Gaussian distribution. The subscript arrows (\rightarrow) show what the expected value will be.

Next, when the depth is $d + 1$,

$$\begin{aligned}
& \mathbb{E}_m \left[f_m^{(d+1)}(\mathbf{x}_i, \mathbf{w}_m, \boldsymbol{\pi}_m) f_m^{(d+1)}(\mathbf{x}_j, \mathbf{w}_m, \boldsymbol{\pi}_m) \right] \\
&= \mathbb{E}_m \left[\left(\sigma(\mathbf{w}_{m,t}^\top \mathbf{x}_i) f_m^{(d)}(\mathbf{x}_i, \mathbf{w}_m^{(l)}, \boldsymbol{\pi}_m^{(l)}) + (1 - \sigma(\mathbf{w}_{m,t}^\top \mathbf{x}_i)) f_m^{(d)}(\mathbf{x}_i, \mathbf{w}_m^{(r)}, \boldsymbol{\pi}_m^{(r)}) \right) \right. \\
&\quad \left. \left(\sigma(\mathbf{w}_{m,t}^\top \mathbf{x}_j) f_m^{(d)}(\mathbf{x}_j, \mathbf{w}_m^{(l)}, \boldsymbol{\pi}_m^{(l)}) + (1 - \sigma(\mathbf{w}_{m,t}^\top \mathbf{x}_j)) f_m^{(d)}(\mathbf{x}_j, \mathbf{w}_m^{(r)}, \boldsymbol{\pi}_m^{(r)}) \right) \right] \\
&= \mathbb{E}_m \left[\left(\underbrace{\left(f_m^{(d)}(\mathbf{x}_i, \mathbf{w}_m^{(l)}, \boldsymbol{\pi}_m^{(l)}) - f_m^{(d)}(\mathbf{x}_i, \mathbf{w}_m^{(r)}, \boldsymbol{\pi}_m^{(r)}) \right) \sigma(\mathbf{w}_{m,t}^\top \mathbf{x}_i)}_{(A)} + \underbrace{f_m^{(d)}(\mathbf{x}_i, \mathbf{w}_m^{(r)}, \boldsymbol{\pi}_m^{(r)})}_{(B)} \right) \right. \\
&\quad \left. \left(\underbrace{\left(f_m^{(d)}(\mathbf{x}_j, \mathbf{w}_m^{(l)}, \boldsymbol{\pi}_m^{(l)}) - f_m^{(d)}(\mathbf{x}_j, \mathbf{w}_m^{(r)}, \boldsymbol{\pi}_m^{(r)}) \right) \sigma(\mathbf{w}_{m,t}^\top \mathbf{x}_j)}_{(C)} + \underbrace{f_m^{(d)}(\mathbf{x}_j, \mathbf{w}_m^{(r)}, \boldsymbol{\pi}_m^{(r)})}_{(D)} \right) \right], \tag{A.20}
\end{aligned}$$

where the last equality sign is just a simplification to separate components (A), (B), (C), and (D). Since $f_m^{(d)}(\mathbf{x}_i, \mathbf{w}_m^{(r)}, \boldsymbol{\pi}_m^{(r)})$ and $f_m^{(d)}(\mathbf{x}_j, \mathbf{w}_m^{(l)}, \boldsymbol{\pi}_m^{(l)})$ are independent to each other and have zero-mean i.i.d Gaussian distribution, we obtain

$$\begin{aligned}
\mathbb{E}_m [(A) \times (C)] &= \mathcal{T}(\mathbf{x}_i, \mathbf{x}_j) \mathbb{E}_m \left[f_m^{(d)}(\mathbf{x}_i, \mathbf{w}_m^{(l)}, \boldsymbol{\pi}_m^{(l)}) f_m^{(d)}(\mathbf{x}_j, \mathbf{w}_m^{(l)}, \boldsymbol{\pi}_m^{(l)}) \right. \\
&\quad \left. + f_m^{(d)}(\mathbf{x}_i, \mathbf{w}_m^{(r)}, \boldsymbol{\pi}_m^{(r)}) f_m^{(d)}(\mathbf{x}_j, \mathbf{w}_m^{(r)}, \boldsymbol{\pi}_m^{(r)}) \right], \tag{A.21}
\end{aligned}$$

$$\mathbb{E}_m [(B) \times (C)] = -0.5 \mathbb{E}_m \left[f_m^{(d)}(\mathbf{x}_i, \mathbf{w}_m^{(r)}, \boldsymbol{\pi}_m^{(r)}) f_m^{(d)}(\mathbf{x}_j, \mathbf{w}_m^{(r)}, \boldsymbol{\pi}_m^{(r)}) \right], \tag{A.22}$$

$$\mathbb{E}_m [(A) \times (D)] = -0.5 \mathbb{E}_m \left[f_m^{(d)}(\mathbf{x}_i, \mathbf{w}_m^{(r)}, \boldsymbol{\pi}_m^{(r)}) f_m^{(d)}(\mathbf{x}_j, \mathbf{w}_m^{(l)}, \boldsymbol{\pi}_m^{(l)}) \right], \tag{A.23}$$

$$\mathbb{E}_m [(B) \times (D)] = \mathbb{E}_m \left[f_m^{(d)}(\mathbf{x}_i, \mathbf{w}_m^{(r)}, \boldsymbol{\pi}_m^{(r)}) f_m^{(d)}(\mathbf{x}_j, \mathbf{w}_m^{(r)}, \boldsymbol{\pi}_m^{(r)}) \right]. \tag{A.24}$$

Equation (A.22), Equation (A.23), and Equation (A.24) cancel each other out. Therefore, we obtain

$$\begin{aligned} & \mathbb{E}_m \left[f_m^{(d+1)}(\mathbf{x}_i, \mathbf{w}_m, \boldsymbol{\pi}_m) f_m^{(d+1)}(\mathbf{x}_j, \mathbf{w}_m, \boldsymbol{\pi}_m) \right] \\ &= 2\mathcal{T}(\mathbf{x}_i, \mathbf{x}_j) \mathbb{E}_m \left[f_m^{(d)}(\mathbf{x}_i, \mathbf{w}_m, \boldsymbol{\pi}_m) f_m^{(d)}(\mathbf{x}_j, \mathbf{w}_m, \boldsymbol{\pi}_m) \right]. \end{aligned} \quad (\text{A.25})$$

By induction hypothesis and Equation (A.18), we have $\mathbb{E}_m \left[f_m^{(d)}(\mathbf{x}_i, \mathbf{w}_m, \boldsymbol{\pi}_m) f_m^{(d)}(\mathbf{x}_j, \mathbf{w}_m, \boldsymbol{\pi}_m) \right] = (2\mathcal{T}(\mathbf{x}_i, \mathbf{x}_j))^d$. Therefore, the original lemma also follows. \square

A.2 Proof of Lemma 2

Proof. When the depth is $d+1$, the derivatives of the parameters in the left subtree and the right subtree are

$$\frac{\partial f^{(d+1)}(\mathbf{x}_i, \mathbf{w}, \boldsymbol{\pi})}{\partial \mathbf{w}_{m,l}} = \sigma(\mathbf{w}_{m,t}^\top \mathbf{x}_i) \frac{\partial f_m^{(d)}(\mathbf{x}_i, \mathbf{w}_m^{(l)}, \boldsymbol{\pi}_m^{(l)})}{\partial \mathbf{w}_{m,l}}, \quad (\text{A.26})$$

$$\frac{\partial f^{(d+1)}(\mathbf{x}_i, \mathbf{w}, \boldsymbol{\pi})}{\partial \mathbf{w}_{m,r}} = (1 - \sigma(\mathbf{w}_{m,t}^\top \mathbf{x}_i)) \frac{\partial f_m^{(d)}(\mathbf{x}_i, \mathbf{w}_m^{(r)}, \boldsymbol{\pi}_m^{(r)})}{\partial \mathbf{w}_{m,r}}, \quad (\text{A.27})$$

where l and r used in $\mathbf{w}_{m,l}$ and $\mathbf{w}_{m,r}$ implies the node at the left subtree and right subtree, respectively. Therefore, the limiting TNTK for the left subtree is

$$\Theta^{(d+1),(l)}(\mathbf{x}_i, \mathbf{x}_j) = \mathcal{T}(\mathbf{x}_i, \mathbf{x}_j) (\Theta^{(d),(t)}(\mathbf{x}_i, \mathbf{x}_j) + \Theta^{(d),(l)}(\mathbf{x}_i, \mathbf{x}_j) + \Theta^{(d),(r)}(\mathbf{x}_i, \mathbf{x}_j)). \quad (\text{A.28})$$

Similarly, for the right subtree, since

$$\begin{aligned} \mathbb{E}[(1 - \sigma(\mathbf{u}^\top \mathbf{x}_i))(1 - \sigma(\mathbf{u}^\top \mathbf{x}_j))] &= \mathbb{E} \left[1 - \underbrace{\sigma(\mathbf{u}^\top \mathbf{x}_i)}_{\rightarrow 0.5} - \underbrace{\sigma(\mathbf{u}^\top \mathbf{x}_j)}_{\rightarrow 0.5} + \sigma(\mathbf{u}^\top \mathbf{x}_i) \sigma(\mathbf{u}^\top \mathbf{x}_j) \right] \\ &= \mathbb{E}[\sigma(\mathbf{u}^\top \mathbf{x}_i) \sigma(\mathbf{u}^\top \mathbf{x}_j)], \end{aligned} \quad (\text{A.29})$$

we can also derive

$$\Theta^{(d+1),(r)}(\mathbf{x}_i, \mathbf{x}_j) = \mathcal{T}(\mathbf{x}_i, \mathbf{x}_j) (\Theta^{(d),(t)}(\mathbf{x}_i, \mathbf{x}_j) + \Theta^{(d),(l)}(\mathbf{x}_i, \mathbf{x}_j) + \Theta^{(d),(r)}(\mathbf{x}_i, \mathbf{x}_j)). \quad (\text{A.30})$$

Finally, we obtain the following by combining with Equation (A.28) and Equation (A.30),

$$\begin{aligned} & \Theta^{(d+1),(l)}(\mathbf{x}_i, \mathbf{x}_j) + \Theta^{(d+1),(r)}(\mathbf{x}_i, \mathbf{x}_j) \\ &= 2\mathcal{T}(\mathbf{x}_i, \mathbf{x}_j) (\Theta^{(d),(t)}(\mathbf{x}_i, \mathbf{x}_j) + \Theta^{(d),(l)}(\mathbf{x}_i, \mathbf{x}_j) + \Theta^{(d),(r)}(\mathbf{x}_i, \mathbf{x}_j)). \end{aligned} \quad (\text{A.31})$$

\square

A.3 Proof of Lemma 3

Proof. With Equation (1) and Equation (6),

$$\begin{aligned} \frac{\partial f(\mathbf{x}_i, \mathbf{w}, \boldsymbol{\pi})}{\partial \pi_{m,\ell}} &= \frac{1}{\sqrt{M}} \mu_{m,\ell}(\mathbf{x}_i, \mathbf{w}_m) \\ &= \frac{1}{\sqrt{M}} \prod_{n=1}^{\mathcal{N}} \sigma(\mathbf{w}_{m,n}^\top \mathbf{x}_i)^{\mathbb{1}_{\ell \prec n}} (1 - \sigma(\mathbf{w}_{m,n}^\top \mathbf{x}_i))^{\mathbb{1}_{n \searrow \ell}}. \end{aligned} \quad (\text{A.32})$$

When we focus on a leaf ℓ , for a tree with depth of d , $\mathbb{1}_{n \searrow \ell}$ or $\mathbb{1}_{\ell \prec n}$ equals to 1 d times. Therefore, by Equation (A.29), we can say that there is a $\mathcal{T}(\mathbf{x}_i, \mathbf{x}_j)^d$ contribution to the limiting kernel $\Theta^{(d),(b)}(\mathbf{x}_i, \mathbf{x}_j)$ per leaf index $\ell \in [\mathcal{L}]$. Since there are 2^d leaf indices in the complete binary tree,

$$\Theta^{(d+1),(b)}(\mathbf{x}_i, \mathbf{x}_j) = (2\mathcal{T}(\mathbf{x}_i, \mathbf{x}_j))^d. \quad (\text{A.33})$$

In other words, since the number of leaves doubles with each additional depth, we can say

$$\Theta^{(d+1),(b)}(\mathbf{x}_i, \mathbf{x}_j) = 2\mathcal{T}(\mathbf{x}_i, \mathbf{x}_j) \Theta^{(d),(b)}(\mathbf{x}_i, \mathbf{x}_j). \quad (\text{A.34})$$

\square

A.4 Closed-form formula for the scaled error function

Since we are using the scaled error function as a decision function defined as

$$\begin{aligned} g_{m,n}(\mathbf{w}_{m,n}, \mathbf{x}_i) &= \sigma(\mathbf{w}_{m,n}^\top \mathbf{x}_i) \\ &= \frac{1}{2} \operatorname{erf}(\alpha \mathbf{w}_{m,n}^\top \mathbf{x}_i) + \frac{1}{2}, \end{aligned} \quad (\text{A.35})$$

\mathcal{T} and $\dot{\mathcal{T}}$ in Theorem 1 can be calculated analytically. Closed-form solutions for the error function (Williams, 1996; Lee et al., 2019) are known to be

$$\mathcal{T}_{\operatorname{erf}}(\mathbf{x}_i, \mathbf{x}_j) := \mathbb{E}[\operatorname{erf}(\mathbf{u}^\top \mathbf{x}_i) \operatorname{erf}(\mathbf{u}^\top \mathbf{x}_j)] = \frac{2}{\pi} \arcsin \left(\frac{\Sigma(\mathbf{x}_i, \mathbf{x}_j)}{\sqrt{(\Sigma(\mathbf{x}_i, \mathbf{x}_i) + 0.5)(\Sigma(\mathbf{x}_j, \mathbf{x}_j) + 0.5)}} \right), \quad (\text{A.36})$$

$$\dot{\mathcal{T}}_{\operatorname{erf}}(\mathbf{x}_i, \mathbf{x}_j) := \mathbb{E}[\dot{\operatorname{erf}}(\mathbf{u}^\top \mathbf{x}_i) \dot{\operatorname{erf}}(\mathbf{u}^\top \mathbf{x}_j)] = \frac{4}{\pi} \frac{1}{\sqrt{(1 + 2\Sigma(\mathbf{x}_i, \mathbf{x}_i))(1 + 2\Sigma(\mathbf{x}_j, \mathbf{x}_j)) - 4\Sigma(\mathbf{x}_i, \mathbf{x}_j)^2}}. \quad (\text{A.37})$$

Using the above equations, we can calculate \mathcal{T} and $\dot{\mathcal{T}}$ with the scaled error function as

$$\begin{aligned} \mathcal{T}(\mathbf{x}_i, \mathbf{x}_j) &= \mathbb{E} \left[\frac{1}{4} \operatorname{erf}(\alpha \mathbf{u}^\top \mathbf{x}_i) \operatorname{erf}(\alpha \mathbf{u}^\top \mathbf{x}_j) \right] + \mathbb{E} \left[\frac{1}{4} \operatorname{erf}(\alpha \mathbf{u}^\top \mathbf{x}_i) + \frac{1}{4} \operatorname{erf}(\alpha \mathbf{u}^\top \mathbf{x}_j) \right] + \frac{1}{4} \\ &= \frac{1}{4} \mathbb{E} [\operatorname{erf}(\alpha \mathbf{u}^\top \mathbf{x}_i) \operatorname{erf}(\alpha \mathbf{u}^\top \mathbf{x}_j)] + \frac{1}{4} \\ &= \frac{1}{2\pi} \arcsin \left(\frac{\alpha^2 \Sigma(\mathbf{x}_i, \mathbf{x}_j)}{\sqrt{(\alpha^2 \Sigma(\mathbf{x}_i, \mathbf{x}_i) + 0.5)(\alpha^2 \Sigma(\mathbf{x}_j, \mathbf{x}_j) + 0.5)}} \right) + \frac{1}{4}, \end{aligned} \quad (\text{A.38})$$

$$\begin{aligned} \dot{\mathcal{T}}(\mathbf{x}_i, \mathbf{x}_j) &= \frac{\alpha^2}{4} \mathbb{E} [\dot{\operatorname{erf}}(\alpha \mathbf{u}^\top \mathbf{x}_i) \dot{\operatorname{erf}}(\alpha \mathbf{u}^\top \mathbf{x}_j)] \\ &= \frac{\alpha^2}{\pi} \frac{1}{\sqrt{(1 + 2\alpha^2 \Sigma(\mathbf{x}_i, \mathbf{x}_i))(1 + 2\alpha^2 \Sigma(\mathbf{x}_j, \mathbf{x}_j)) - 4\alpha^4 \Sigma(\mathbf{x}_i, \mathbf{x}_j)^2}}. \end{aligned} \quad (\text{A.39})$$

B Proof of Theorem 2

Proof. We can use the same approach with the proof of Theorem 1. An incremental formula of the output from the oblivious tree ensemble is as follows:

$$\begin{aligned} f^{(d)}(\mathbf{x}_i, \mathbf{w}, \boldsymbol{\pi}) &= \frac{1}{\sqrt{M}} \sum_{m=1}^M \left(\sigma(\mathbf{w}_{m,t}^\top \mathbf{x}_i) f_m^{(d-1)}(\mathbf{x}_i, \mathbf{w}_m^{(s)}, \boldsymbol{\pi}_m^{(l)}) \right. \\ &\quad \left. + (1 - \sigma(\mathbf{w}_{m,t}^\top \mathbf{x}_i)) f_m^{(d-1)}(\mathbf{x}_i, \mathbf{w}_m^{(s)}, \boldsymbol{\pi}_m^{(r)}) \right). \end{aligned} \quad (\text{B.1})$$

Intuitively, the fundamental of Theorem 2 is that the outputs of the left subtree and right subtree are still independent with oblivious tree structure. Even with parameter sharing at the same depth, since the leaf parameters $\boldsymbol{\pi}$ are not shared, the outputs of the left subtree and right subtree are independent.

We will see that Lemma 1, 2 and 3 are also valid for oblivious tree ensembles.

Correspondence to Lemma 1 To show the correspondence to Lemma 1, it is sufficient to show that Equation (A.21), Equation (A.22), Equation (A.23), and Equation (A.24) hold when

$$\begin{aligned} & \mathbb{E}_m \left[f_m^{(d+1)}(\mathbf{x}_i, \mathbf{w}_m, \boldsymbol{\pi}_m) f_m^{(d+1)}(\mathbf{x}_j, \mathbf{w}_m, \boldsymbol{\pi}_m) \right] \\ &= \mathbb{E}_m \left[\left(\underbrace{\left(f_m^{(d)}(\mathbf{x}_i, \mathbf{w}_m^{(s)}, \boldsymbol{\pi}_m^{(l)}) - f_m^{(d)}(\mathbf{x}_i, \mathbf{w}_m^{(s)}, \boldsymbol{\pi}_m^{(r)}) \right) \sigma(\mathbf{w}_{m,t}^\top \mathbf{x}_i)}_{(A)} + \underbrace{f_m^{(d)}(\mathbf{x}_i, \mathbf{w}_m^{(s)}, \boldsymbol{\pi}_m^{(r)})}_{(B)} \right) \right. \\ & \quad \left. \left(\underbrace{\left(f_m^{(d)}(\mathbf{x}_j, \mathbf{w}_m^{(s)}, \boldsymbol{\pi}_m^{(l)}) - f_m^{(d)}(\mathbf{x}_j, \mathbf{w}_m^{(s)}, \boldsymbol{\pi}_m^{(r)}) \right) \sigma(\mathbf{w}_{m,t}^\top \mathbf{x}_j)}_{(C)} + \underbrace{f_m^{(d)}(\mathbf{x}_j, \mathbf{w}_m^{(s)}, \boldsymbol{\pi}_m^{(r)})}_{(D)} \right) \right]. \end{aligned} \quad (\text{B.2})$$

This equation corresponds to Equation (A.20). Here, since the leaf parameters $\boldsymbol{\pi}$ are not shared, the outputs of the left subtree and right subtree are still independent even with the oblivious tree structure. Therefore, we can obtain the correspondences to Equation (A.21), Equation (A.22), Equation (A.23), and Equation (A.24) with the same procedures.

Correspondence to Lemma 2 For the depth $d + 1$, since

$$\begin{aligned} \frac{\partial f_m^{(d+1)}(\mathbf{x}_i, \mathbf{w}, \boldsymbol{\pi})}{\partial \mathbf{w}_{m,s}} &= \sigma(\mathbf{w}_{m,t}^\top \mathbf{x}_i) \frac{\partial f_m^{(d)}(\mathbf{x}_i, \mathbf{w}_m^{(s)}, \boldsymbol{\pi}_m^{(r)})}{\partial \mathbf{w}_{m,s}} \\ &+ (1 - \sigma(\mathbf{w}_{m,t}^\top \mathbf{x}_i)) \frac{\partial f_m^{(d)}(\mathbf{x}_i, \mathbf{w}_m^{(s)}, \boldsymbol{\pi}_m^{(l)})}{\partial \mathbf{w}_{m,s}}, \end{aligned} \quad (\text{B.3})$$

the corresponding limiting TNTK is

$$\begin{aligned} & \Theta^{(d+1),(s)}(\mathbf{x}_i, \mathbf{x}_j) \\ &= \sum_{s=2}^d \mathbb{E}_m \left[\left(\sigma(\mathbf{w}_{m,t}^\top \mathbf{x}_i) \frac{\partial f_m^{(d)}(\mathbf{x}_i, \mathbf{w}_m^{(s)}, \boldsymbol{\pi}_m^{(r)})}{\partial \mathbf{w}_{m,s}} + (1 - \sigma(\mathbf{w}_{m,t}^\top \mathbf{x}_i)) \frac{\partial f_m^{(d)}(\mathbf{x}_i, \mathbf{w}_m^{(s)}, \boldsymbol{\pi}_m^{(l)})}{\partial \mathbf{w}_{m,s}} \right)^\top \right. \\ & \quad \left. \left(\sigma(\mathbf{w}_{m,t}^\top \mathbf{x}_j) \frac{\partial f_m^{(d)}(\mathbf{x}_j, \mathbf{w}_m^{(s)}, \boldsymbol{\pi}_m^{(r)})}{\partial \mathbf{w}_{m,s}} + (1 - \sigma(\mathbf{w}_{m,t}^\top \mathbf{x}_j)) \frac{\partial f_m^{(d)}(\mathbf{x}_j, \mathbf{w}_m^{(s)}, \boldsymbol{\pi}_m^{(l)})}{\partial \mathbf{w}_{m,s}} \right) \right] \\ &= \sum_{s=2}^d \mathbb{E}_m \left[\left(\underbrace{\sigma(\mathbf{w}_{m,t}^\top \mathbf{x}_i) \left(\frac{\partial f_m^{(d)}(\mathbf{x}_i, \mathbf{w}_m^{(s)}, \boldsymbol{\pi}_m^{(l)})}{\partial \mathbf{w}_{m,s}} - \frac{\partial f_m^{(d)}(\mathbf{x}_i, \mathbf{w}_m^{(s)}, \boldsymbol{\pi}_m^{(r)})}{\partial \mathbf{w}_{m,s}} \right)}_{(A)} + \underbrace{\frac{\partial f_m^{(d)}(\mathbf{x}_i, \mathbf{w}_m^{(s)}, \boldsymbol{\pi}_m^{(r)})}{\partial \mathbf{w}_{m,s}}}_{(B)} \right)^\top \right. \\ & \quad \left. \left(\underbrace{\sigma(\mathbf{w}_{m,t}^\top \mathbf{x}_j) \left(\frac{\partial f_m^{(d)}(\mathbf{x}_j, \mathbf{w}_m^{(s)}, \boldsymbol{\pi}_m^{(l)})}{\partial \mathbf{w}_{m,s}} - \frac{\partial f_m^{(d)}(\mathbf{x}_j, \mathbf{w}_m^{(s)}, \boldsymbol{\pi}_m^{(r)})}{\partial \mathbf{w}_{m,s}} \right)}_{(C)} + \underbrace{\frac{\partial f_m^{(d)}(\mathbf{x}_j, \mathbf{w}_m^{(s)}, \boldsymbol{\pi}_m^{(r)})}{\partial \mathbf{w}_{m,s}}}_{(D)} \right) \right]. \end{aligned} \quad (\text{B.4})$$

Since $\frac{\partial f_m^{(d)}(\mathbf{x}_i, \mathbf{w}_m^{(s)}, \boldsymbol{\pi}_m^{(r)})}{\partial \mathbf{w}_{m,s}}$ and $\frac{\partial f_m^{(d)}(\mathbf{x}_j, \mathbf{w}_m^{(s)}, \boldsymbol{\pi}_m^{(l)})}{\partial \mathbf{w}_{m,s}}$ for $s = \{2, 3, \dots, d\}$ are independent to each other and have zero-mean Gaussian distribution³, similar calculation used for Equation (A.21), Equ-

³For a single oblivious tree, the number splitting rule is d because of the parameter sharing.

tion (A.22), Equation (A.23), and Equation (A.24) gives

$$\begin{aligned} \mathbb{E}_m[(A) \times (C)] &= \mathcal{T}(\mathbf{x}_i, \mathbf{x}_j) \mathbb{E}_m \left[\left(\frac{\partial f_m^{(d)}(\mathbf{x}_i, \mathbf{w}_m^{(s)}, \boldsymbol{\pi}_m^{(l)})}{\partial \mathbf{w}_{m,s}} \right)^\top \left(\frac{\partial f_m^{(d)}(\mathbf{x}_j, \mathbf{w}_m^{(s)}, \boldsymbol{\pi}_m^{(l)})}{\partial \mathbf{w}_{m,s}} \right) \right. \\ &\quad \left. + \left(\frac{\partial f_m^{(d)}(\mathbf{x}_i, \mathbf{w}_m^{(s)}, \boldsymbol{\pi}_m^{(r)})}{\partial \mathbf{w}_{m,s}} \right)^\top \left(\frac{\partial f_m^{(d)}(\mathbf{x}_j, \mathbf{w}_m^{(s)}, \boldsymbol{\pi}_m^{(r)})}{\partial \mathbf{w}_{m,s}} \right) \right], \end{aligned} \quad (\text{B.5})$$

$$\mathbb{E}_m[(B) \times (C)] = -0.5 \mathbb{E}_m \left[\left(\frac{\partial f_m^{(d)}(\mathbf{x}_i, \mathbf{w}_m^{(s)}, \boldsymbol{\pi}_m^{(r)})}{\partial \mathbf{w}_{m,s}} \right)^\top \left(\frac{\partial f_m^{(d)}(\mathbf{x}_j, \mathbf{w}_m^{(s)}, \boldsymbol{\pi}_m^{(r)})}{\partial \mathbf{w}_{m,s}} \right) \right], \quad (\text{B.6})$$

$$\mathbb{E}_m[(A) \times (D)] = -0.5 \mathbb{E}_m \left[\left(\frac{\partial f_m^{(d)}(\mathbf{x}_i, \mathbf{w}_m^{(s)}, \boldsymbol{\pi}_m^{(r)})}{\partial \mathbf{w}_{m,s}} \right)^\top \left(\frac{\partial f_m^{(d)}(\mathbf{x}_j, \mathbf{w}_m^{(s)}, \boldsymbol{\pi}_m^{(r)})}{\partial \mathbf{w}_{m,s}} \right) \right], \quad (\text{B.7})$$

$$\mathbb{E}_m[(B) \times (D)] = \mathbb{E}_m \left[\left(\frac{\partial f_m^{(d)}(\mathbf{x}_i, \mathbf{w}_m^{(s)}, \boldsymbol{\pi}_m^{(r)})}{\partial \mathbf{w}_{m,s}} \right)^\top \left(\frac{\partial f_m^{(d)}(\mathbf{x}_j, \mathbf{w}_m^{(s)}, \boldsymbol{\pi}_m^{(r)})}{\partial \mathbf{w}_{m,s}} \right) \right]. \quad (\text{B.8})$$

As in the previous calculations, Equation (B.6), Equation (B.7), and Equation (B.8) cancel each other out. As a result, we obtain

$$\Theta^{(d+1),(s)}(\mathbf{x}_i, \mathbf{x}_j) = 2\mathcal{T}(\mathbf{x}_i, \mathbf{x}_j) \left(\Theta^{(d),(t)}(\mathbf{x}_i, \mathbf{x}_j) + \Theta^{(d),(s)}(\mathbf{x}_i, \mathbf{x}_j) \right). \quad (\text{B.9})$$

Correspondence to Lemma 3 Considering Equation (A.32), once we focus on a leaf ℓ , it is not possible for both $\mathbb{1}_{1 \searrow \ell}$ and $\mathbb{1}_{\ell \swarrow 1}$ to be 1. This means that a leaf cannot belong to both the right subtree and the left subtree. Therefore, even with oblivious tree structure, there is no influences. Therefore, we get exactly the same result to the Lemma 3. \square

C Proof of Proposition 1

Proof. As shown in Section 4.1, there is a close correspondence between the soft tree ensemble of depth 1 and the two-layer perceptron. On the one hand, from Equation (A.6), the limiting TNTK induced by infinite trees with the depth of 1 is $2(\Sigma(\mathbf{x}_i, \mathbf{x}_j)\dot{\mathcal{T}}(\mathbf{x}_i, \mathbf{x}_j) + \mathcal{T}(\mathbf{x}_i, \mathbf{x}_j))$. On the other hand, if the activation function used in the two-layer perceptron is same as σ defined in Equation (5), the NTK induced by the infinite width two-layer MLP is $\Sigma(\mathbf{x}_i, \mathbf{x}_j)\dot{\mathcal{T}}(\mathbf{x}_i, \mathbf{x}_j) + \mathcal{T}(\mathbf{x}_i, \mathbf{x}_j)$ (Jacot et al., 2018; Lee et al., 2019). Hence these are exactly the same kernel up to constant multiple.

The conditions under which the MLP-induced NTK are positively definite have already been studied.

Lemma 4 (Jacot et al. (2018)). *For a non-polynomial Lipschitz nonlinearity σ , for any input dimension N_0 , the NTK induced by the infinite width MLP is positive definite if $\|\mathbf{x}_i\|_2 = 1$ for all $i \in [N]$ and $\mathbf{x}_i \neq \mathbf{x}_j$ ($i \neq j$).*

Note that σ defined in Equation (5) has the non-polynomial Lipschitz nonlinearity. Since the positive definite kernel multiplied by a constant is a positive definite kernel, it follows that the limiting TNTK $\Theta^{(1)}(\mathbf{x}_i, \mathbf{x}_j)$ for the depth 1 is also positive definite.

As shown in Equation (C.1), as the trees get deeper, $\mathcal{T}(\mathbf{x}_i, \mathbf{x}_j)$ defined in Equation (9) is multiplied multiple times in the limiting TNTK:

$$\begin{aligned} \Theta^{(d)}(\mathbf{x}_i, \mathbf{x}_j) &= \underbrace{d(2^d)\Sigma(\mathbf{x}_i, \mathbf{x}_j)(\mathcal{T}(\mathbf{x}_i, \mathbf{x}_j))^{d-1}\dot{\mathcal{T}}(\mathbf{x}_i, \mathbf{x}_j)}_{\text{contribution from inner nodes}} + \underbrace{(2\mathcal{T}(\mathbf{x}_i, \mathbf{x}_j))^d}_{\text{contribution from leaves}} \\ &= 2(2\mathcal{T}(\mathbf{x}_i, \mathbf{x}_j))^{d-1} \underbrace{(d\Sigma(\mathbf{x}_i, \mathbf{x}_j)\dot{\mathcal{T}}(\mathbf{x}_i, \mathbf{x}_j) + \mathcal{T}(\mathbf{x}_i, \mathbf{x}_j))}_{\text{NTK induced by two-layer perceptron (if } d=1)}. \end{aligned} \quad (\text{C.1})$$

The positive definiteness of $\mathcal{T}(\mathbf{x}_i, \mathbf{x}_j)$ has already been proven.

Lemma 5 (Jacot et al. (2018)). *For a non-polynomial Lipschitz nonlinearity σ , for any input dimension N_0 , the $\mathcal{T}(\mathbf{x}_i, \mathbf{x}_j) := \mathbb{E}[\sigma(\mathbf{u}^\top \mathbf{x}_i)\sigma(\mathbf{u}^\top \mathbf{x}_j)]$ defined in Theorem 1 is positive definite if $\|\mathbf{x}_i\|_2 = 1$ for all $i \in [N]$ and $\mathbf{x}_i \neq \mathbf{x}_j$ ($i \neq j$).*

Note that $d\Sigma(\mathbf{x}_i, \mathbf{x}_j)\dot{\mathcal{T}}(\mathbf{x}_i, \mathbf{x}_j) + \mathcal{T}(\mathbf{x}_i, \mathbf{x}_j)$ for $d \in \mathbb{N}$ is positive definite. Since the product of the positive definite kernel is positive definite, for infinite trees of arbitrary depth, the positive definiteness of $\Theta^{(d)}(\mathbf{x}_i, \mathbf{x}_j)$ holds under the same conditions as in MLP. \square

D Proof of Theorem 3

Proof. We use the following lemmas in the proof.

Lemma 6. *Let $\mathbf{a} \in \mathbb{R}^n$ be a random vector whose entries are independent standard normal random variables. For every $v \geq 0$, with probability at least $1 - 2^n e^{(-v^2 n/2)}$ we have:*

$$\|\mathbf{a}\|_1 \leq vn. \quad (\text{D.1})$$

Lemma 7. *Let $a_i \in \mathbb{R}$ be an arbitrary real number. We have*

$$\sum_{i=1}^n \sqrt{a_i} \leq \sqrt{n} \sqrt{\sum_{i=1}^n a_i}. \quad (\text{D.2})$$

In addition, our proof is based on the strategy used in Lee et al. (2019) which relies on the the local Lipschitzness of the model Jacobian at initialization $\mathbf{J}(\mathbf{x}, \boldsymbol{\theta})$, whose (i, j) entry is $\frac{\partial f(\mathbf{x}_i, \boldsymbol{\theta})}{\partial \theta_j}$ where θ_j is a j -th component of $\boldsymbol{\theta}$:

Theorem 4 (Lee et al. (2019)). *Assume that the limiting NTK induced by any model architecture is positive definite for input sets \mathbf{x} such that minimum eigenvalue of the NTK $\lambda_{\min} > 0$. For models with local Lipschitz Jacobian trained under gradient flow with a learning rate $\eta < 2(\lambda_{\min} + \lambda_{\max})$, we have with high probability:*

$$\sup \left| \hat{\Theta}_\tau^*(\mathbf{x}_i, \mathbf{x}_j) - \hat{\Theta}_0^*(\mathbf{x}_i, \mathbf{x}_j) \right| = \mathcal{O} \left(\frac{1}{\sqrt{M}} \right). \quad (\text{D.3})$$

It is not obvious whether or not the soft tree ensemble's Jacobian is local Lipschitz. Therefore, we prove Lemma 8 to prove Theorem 3.

Lemma 8. *For soft tree ensemble models with the NTK initialization and a positive finite scaling factor α , there is $K > 0$ such that for every $C > 0$, with high probability, the following holds:*

$$\begin{cases} \|\mathbf{J}(\mathbf{x}, \boldsymbol{\theta})\|_F & \leq K \\ \|\mathbf{J}(\mathbf{x}, \boldsymbol{\theta}) - \mathbf{J}(\mathbf{x}, \tilde{\boldsymbol{\theta}})\|_F & \leq K \|\boldsymbol{\theta} - \tilde{\boldsymbol{\theta}}\|_2 \end{cases}, \forall \boldsymbol{\theta}, \tilde{\boldsymbol{\theta}} \in B(\boldsymbol{\theta}_0, C), \quad (\text{D.4})$$

where

$$B(\boldsymbol{\theta}_0, C) := \{\boldsymbol{\theta} : \|\boldsymbol{\theta} - \boldsymbol{\theta}_0\|_2 < C\}. \quad (\text{D.5})$$

By proving that the soft tree ensemble's Jacobian under the NTK initialization is the local Lipschitz with high probability, we extend the Theorem 3 for the TNTK. \square

D.1 Proof of Lemma 6

Proof. By use of the Chebyshev's inequality, for some constant c , we obtain

$$\begin{aligned} P(\|\mathbf{a}\|_1 > c) & \leq \mathbb{E}[e^{\gamma \|\mathbf{a}\|_1}] / e^{\gamma c} \\ & = \left(e^{\gamma^2/2} (1 + \text{erf}(\gamma/\sqrt{2})) \right)^n / e^{\gamma c}, \end{aligned} \quad (\text{D.6})$$

where P means a probability. Since $\text{erf}(\gamma/\sqrt{2}) \leq 1$, when we use $\gamma = c/n$, we get

$$P(\|\mathbf{a}\|_1 > c) \leq 2^n e^{(-c^2/2n)}. \quad (\text{D.7})$$

Lemma 6 can be obtained by assigning vn to c . \square

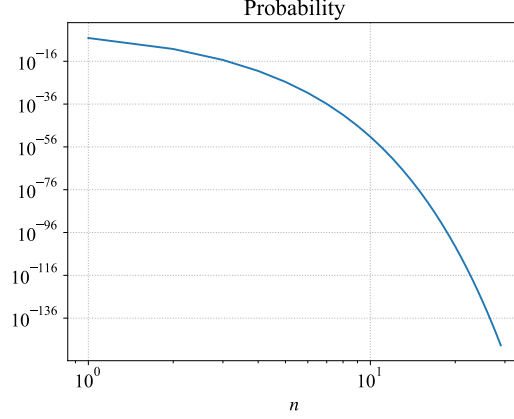


Figure 7: Right hand side of the Equation (D.7), where $c = 5n$ (in other words, $v = 5$ in Lemma 6).

Figure 7 shows the right hand side of the Equation (D.7) with $c = 5n$. when $n = 1$, probability is 7.45×10^{-6} . As n becomes larger, the probability becomes even smaller.

D.2 Proof of Lemma 7

Proof. By use of Cauchy-Schwarz inequality, for $p, q, x, y \in \mathbb{R}$, we have

$$p\sqrt{x} + q\sqrt{y} \leq \sqrt{(a^2 + b^2)(x + y)}. \quad (\text{D.8})$$

With Equation (D.8), we prove the lemma by induction. In the base case,

$$\sqrt{a_1} + \sqrt{a_2} \leq \sqrt{2}\sqrt{a_1 + a_2}, \quad (\text{D.9})$$

which is consistent to the lemma. Next, when we assume

$$\sqrt{a_1} + \dots + \sqrt{a_k} \leq \sqrt{k}\sqrt{a_1 + \dots + a_k}, \quad (\text{D.10})$$

we have

$$\begin{aligned} \sqrt{a_1} + \dots + \sqrt{a_k} + \sqrt{a_{k+1}} &= (\sqrt{a_1} + \dots + \sqrt{a_k}) + \sqrt{a_{k+1}} \\ &\leq \sqrt{k}\sqrt{a_1 + \dots + a_k} + \sqrt{a_{k+1}} \\ &\leq \sqrt{k+1}\sqrt{a_1 + \dots + a_k + a_{k+1}}. \end{aligned} \quad (\text{D.11})$$

□

D.3 Proof of Lemma 8

Proof. Consider the contribution of the leaf parameters at first:

$$\frac{\partial f(\mathbf{x}_i, \mathbf{w}, \boldsymbol{\pi})}{\partial \pi_{m,\ell}} = \frac{1}{\sqrt{M}} \mu_{m,\ell}(\mathbf{x}_i, \mathbf{w}_m). \quad (\text{D.12})$$

Next, contribution from the leaf parameters is

$$\begin{aligned} \frac{\partial f(\mathbf{x}_i, \mathbf{w}, \boldsymbol{\pi})}{\partial \mathbf{w}_{m,n}} &= \frac{1}{\sqrt{M}} \sum_{\ell=1}^{\mathcal{L}} \pi_{m,\ell} \frac{\partial \mu_{m,\ell}(\mathbf{x}_i, \mathbf{w}_m)}{\partial \mathbf{w}_{m,n}} \\ &= \frac{1}{\sqrt{M}} \sum_{\ell=1}^{\mathcal{L}} \pi_{m,\ell} S_{n,\ell}(\mathbf{x}_i, \mathbf{w}_m) \mathbf{x}_i \dot{\sigma}(\mathbf{w}_{m,n}^\top \mathbf{x}_i), \end{aligned} \quad (\text{D.13})$$

where

$$S_{n,\ell}(\mathbf{x}, \mathbf{w}_m) := \left(\prod_{n'=1}^{\mathcal{N}} \sigma(\mathbf{w}_{m,n'}^\top \mathbf{x}_i)^{\mathbb{1}_{(\ell \prec n') \& (n \neq n')}} (1 - \sigma(\mathbf{w}_{m,n'}^\top \mathbf{x}_i))^{\mathbb{1}_{(n' \succ \ell) \& (n \neq n')}} \right) (-1)^{\mathbb{1}_{n \succ \ell}}, \quad (\text{D.14})$$

and $\&$ is a logical conjunction. For any real scalar p and q , the scaled error function σ defined in Equation (5) is bounded as follows:

$$0 \leq \sigma(p) \leq 1, \quad |\sigma(p) - \sigma(q)| \leq |p - q|, \quad 0 \leq \dot{\sigma}(p) \leq \alpha, \quad |\dot{\sigma}(p) - \dot{\sigma}(q)| \leq \alpha|p - q|. \quad (\text{D.15})$$

Therefore, the absolute value of $S_{n,\ell}$ does not exceed 1. With Equation (D.15), we can obtain

$$\left\| \frac{\partial \mu_{m,\ell}(\mathbf{x}_i, \mathbf{w}_m)}{\partial \mathbf{w}_{m,n}} \right\|_2 = \|S_{n,\ell}(\mathbf{x}_i, \mathbf{w}_m) \mathbf{x}_i \dot{\sigma}(\mathbf{w}_{m,n}^\top \mathbf{x}_i)\|_2 \leq \alpha \|\mathbf{x}_i\|_2 \quad (\text{D.16})$$

with high probability. Therefore, with Lemma 6, in probability,

$$\begin{aligned} \|\mathbf{J}(\mathbf{x}, \boldsymbol{\theta})\|_F^2 &= \sum_{i=1}^N (\|\mathbf{J}(\mathbf{x}_i, \mathbf{w})\|_F^2 + \|\mathbf{J}(\mathbf{x}_i, \boldsymbol{\pi})\|_F^2) \\ &= \frac{1}{M} \sum_{i=1}^N \sum_{m=1}^M \left(\sum_{n=1}^{\mathcal{N}} \left(\left\| \sum_{\ell=1}^{\mathcal{L}} \pi_{m,\ell} \frac{\partial \mu_{m,\ell}(\mathbf{x}_i, \mathbf{w}_m)}{\partial \mathbf{w}_{m,n}} \right\|_2^2 \right) + \sum_{\ell=1}^{\mathcal{L}} (\mu_{m,\ell}(\mathbf{x}_i, \mathbf{w}_m)^2) \right) \\ &\leq \frac{1}{M} \sum_{i=1}^N \sum_{m=1}^M \left(\sum_{n=1}^{\mathcal{N}} v^2 \mathcal{L}^2 \alpha^2 \|\mathbf{x}_i\|_2^2 + \sum_{\ell=1}^{\mathcal{L}} 1 \right) \\ &= \sum_{i=1}^N \mathcal{L}(v^2 \mathcal{L} \alpha^2 \mathcal{N} \|\mathbf{x}_i\|_2^2 + 1). \end{aligned} \quad (\text{D.17})$$

Next, we will consider the Jacobian difference. Since $\mu_{m,\ell}(\mathbf{x}_i, \mathbf{w}_m)$ is a multiple multiplication of the decision function, by use of

$$\left| \prod_{i=1}^n p_i - \prod_{i=1}^n q_i \right| \leq \sum_{i=1}^n |p_i - q_i| \quad \text{for } |p_i|, |q_i| \leq 1, \quad (\text{D.18})$$

we obtain

$$\begin{aligned} |\mu_{m,\ell}(\mathbf{x}_i, \mathbf{w}_m) - \mu_{m,\ell}(\mathbf{x}_i, \tilde{\mathbf{w}}_m)| &= \left| \prod_{n=1}^{\mathcal{N}} \sigma(\mathbf{w}_{m,n}^\top \mathbf{x}_i)^{\mathbb{1}_{\ell \swarrow n}} (1 - \sigma(\mathbf{w}_{m,n}^\top \mathbf{x}_i))^{\mathbb{1}_{n \searrow \ell}} \right. \\ &\quad \left. - \prod_{n=1}^{\mathcal{N}} \sigma(\tilde{\mathbf{w}}_{m,n}^\top \mathbf{x}_i)^{\mathbb{1}_{\ell \swarrow n}} (1 - \sigma(\tilde{\mathbf{w}}_{m,n}^\top \mathbf{x}_i))^{\mathbb{1}_{n \searrow \ell}} \right| \\ &\leq \sum_{n=1}^{\mathcal{N}} \left| \sigma(\mathbf{w}_{m,n}^\top \mathbf{x}_i)^{\mathbb{1}_{\ell \swarrow n}} (1 - \sigma(\mathbf{w}_{m,n}^\top \mathbf{x}_i))^{\mathbb{1}_{n \searrow \ell}} \right. \\ &\quad \left. - \sigma(\tilde{\mathbf{w}}_{m,n}^\top \mathbf{x}_i)^{\mathbb{1}_{\ell \swarrow n}} (1 - \sigma(\tilde{\mathbf{w}}_{m,n}^\top \mathbf{x}_i))^{\mathbb{1}_{n \searrow \ell}} \right| \\ &\leq \sum_{n=1}^{\mathcal{N}} |\mathbf{w}_{m,n}^\top \mathbf{x}_i - \tilde{\mathbf{w}}_{m,n}^\top \mathbf{x}_i| \\ &\leq \sum_{n=1}^{\mathcal{N}} \|\mathbf{x}_i\|_2 \|\mathbf{w}_{m,n} - \tilde{\mathbf{w}}_{m,n}\|_2, \end{aligned} \quad (\text{D.19})$$

where it should be noted that $(\ell \swarrow n) \& (n \searrow \ell)$ must be false.

$S_{n,\ell}(\mathbf{x}_i, \mathbf{w}_m) - S_{n,\ell}(\mathbf{x}_i, \tilde{\mathbf{w}}_m)$ can be bound in the same way as Equation (D.19). Therefore, we also obtain

$$\begin{aligned}
\left\| \frac{\partial \mu_{m,\ell}(\mathbf{x}_i, \mathbf{w}_m)}{\partial \mathbf{w}_{m,n}} - \frac{\partial \mu_{m,\ell}(\mathbf{x}_i, \tilde{\mathbf{w}}_m)}{\partial \tilde{\mathbf{w}}_{m,n}} \right\|_2 &= \|S_{n,\ell}(\mathbf{x}_i, \mathbf{w}_m) \mathbf{x}_i \dot{\sigma}(\mathbf{w}_{m,n}^\top \mathbf{x}_i) - S_{n,\ell}(\mathbf{x}_i, \tilde{\mathbf{w}}_m) \mathbf{x}_i \dot{\sigma}(\tilde{\mathbf{w}}_{m,n}^\top \mathbf{x}_i)\|_2 \\
&= \|\mathbf{x}_i\|_2 |S_{n,\ell}(\mathbf{x}_i, \mathbf{w}_m) \dot{\sigma}(\mathbf{w}_{m,n}^\top \mathbf{x}_i) - S_{n,\ell}(\mathbf{x}_i, \tilde{\mathbf{w}}_m) \dot{\sigma}(\tilde{\mathbf{w}}_{m,n}^\top \mathbf{x}_i)| \\
&\leq \|\mathbf{x}_i\|_2 \left(|(S_{n,\ell}(\mathbf{x}_i, \mathbf{w}_m) - S_{n,\ell}(\mathbf{x}_i, \tilde{\mathbf{w}}_m)) \dot{\sigma}(\mathbf{w}_{m,n}^\top \mathbf{x}_i)| \right. \\
&\quad \left. + |(\dot{\sigma}(\mathbf{w}_{m,n}^\top \mathbf{x}_i) - \dot{\sigma}(\tilde{\mathbf{w}}_{m,n}^\top \mathbf{x}_i)) S_{n,\ell}(\mathbf{x}_i, \tilde{\mathbf{w}}_m)| \right) \\
&\leq \|\mathbf{x}_i\|_2 \left(|\alpha(S_{n,\ell}(\mathbf{x}_i, \mathbf{w}_m) - S_{n,\ell}(\mathbf{x}_i, \tilde{\mathbf{w}}_m))| \right. \\
&\quad \left. + |(\alpha(\mathbf{w}_{m,n}^\top \mathbf{x}_i - \tilde{\mathbf{w}}_{m,n}^\top \mathbf{x}_i))| \right) \\
&\leq 2\alpha \|\mathbf{x}_i\|_2^2 \sum_{n=1}^{\mathcal{N}} \|\mathbf{w}_{m,n} - \tilde{\mathbf{w}}_{m,n}\|_2. \tag{D.20}
\end{aligned}$$

To link Equation (D.19) and Equation (D.20) to the $\|\boldsymbol{\theta} - \tilde{\boldsymbol{\theta}}\|_2$, we use Lemma 7 to obtain the following inequalities:

$$\sum_{n=1}^{\mathcal{N}} \|\mathbf{w}_{m,n} - \tilde{\mathbf{w}}_{m,n}\|_2 \leq \sqrt{\mathcal{N}} \|\mathbf{w}_m - \tilde{\mathbf{w}}_m\|_2 \leq \sqrt{\mathcal{N}} \|\boldsymbol{\theta} - \tilde{\boldsymbol{\theta}}\|_2, \tag{D.21}$$

$$\sum_{\ell=1}^{\mathcal{L}} |\pi_{m,\ell} - \tilde{\pi}_{m,\ell}| \leq \sqrt{\mathcal{L}} \|\boldsymbol{\pi}_m - \tilde{\boldsymbol{\pi}}_m\|_2 \leq \sqrt{\mathcal{L}} \|\boldsymbol{\theta} - \tilde{\boldsymbol{\theta}}\|_2. \tag{D.22}$$

With Equation (D.1), Equation (D.16), Equation (D.19), Equation (D.20), Equation (D.21), and Equation (D.22),

$$\begin{aligned}
&\|\mathbf{J}(\mathbf{x}, \boldsymbol{\theta}) - \mathbf{J}(\mathbf{x}, \tilde{\boldsymbol{\theta}})\|_F^2 \\
&= \sum_{i=1}^N (\|\mathbf{J}(\mathbf{x}_i, \mathbf{w}) - \mathbf{J}(\mathbf{x}_i, \tilde{\mathbf{w}})\|_F^2 + \|\mathbf{J}(\mathbf{x}_i, \boldsymbol{\pi}) - \mathbf{J}(\mathbf{x}_i, \tilde{\boldsymbol{\pi}})\|_F^2) \\
&= \frac{1}{M} \sum_{i=1}^N \sum_{m=1}^M \left(\sum_{n=1}^{\mathcal{N}} \left(\left\| \sum_{\ell=1}^{\mathcal{L}} \left(\pi_{m,\ell} \frac{\partial \mu_{m,\ell}(\mathbf{x}_i, \mathbf{w}_m)}{\partial \mathbf{w}_{m,n}} - \tilde{\pi}_{m,\ell} \frac{\partial \mu_{m,\ell}(\mathbf{x}_i, \tilde{\mathbf{w}}_m)}{\partial \tilde{\mathbf{w}}_{m,n}} \right) \right\|_2^2 \right. \right. \\
&\quad \left. \left. + \sum_{\ell=1}^{\mathcal{L}} (\mu_{m,\ell}(\mathbf{x}_i, \mathbf{w}_m) - \mu_{m,\ell}(\mathbf{x}_i, \tilde{\mathbf{w}}_m))^2 \right) \right) \\
&= \frac{1}{M} \sum_{i=1}^N \sum_{m=1}^M \left(\sum_{n=1}^{\mathcal{N}} \left(\left\| \sum_{\ell=1}^{\mathcal{L}} \left((\pi_{m,\ell} - \tilde{\pi}_{m,\ell}) \frac{\partial \mu_{m,\ell}(\mathbf{x}_i, \mathbf{w}_m)}{\partial \mathbf{w}_{m,n}} + \left(\frac{\partial \mu_{m,\ell}(\mathbf{x}_i, \mathbf{w}_m)}{\partial \mathbf{w}_{m,n}} - \frac{\partial \mu_{m,\ell}(\mathbf{x}_i, \tilde{\mathbf{w}}_m)}{\partial \tilde{\mathbf{w}}_{m,n}} \right) \tilde{\pi}_{m,\ell} \right) \right\|_2^2 \right. \right. \\
&\quad \left. \left. + \sum_{\ell=1}^{\mathcal{L}} (\mu_{m,\ell}(\mathbf{x}_i, \mathbf{w}_m) - \mu_{m,\ell}(\mathbf{x}_i, \tilde{\mathbf{w}}_m))^2 \right) \right)
\end{aligned}$$

$$\begin{aligned}
&\leq \frac{1}{M} \sum_{i=1}^N \sum_{m=1}^M \left(\sum_{n=1}^{\mathcal{N}} \left(\left(\sum_{\ell=1}^{\mathcal{L}} (|\pi_{m,\ell} - \tilde{\pi}_{m,\ell}| \alpha \|\mathbf{x}_i\|_2) + \left(2\alpha \|\mathbf{x}_i\|_2^2 \sum_{n=1}^{\mathcal{N}} \|\mathbf{w}_{m,n} - \tilde{\mathbf{w}}_{m,n}\|_2 v \mathcal{L} \right) \right) \right)^2 \right. \\
&\quad \left. + \sum_{\ell=1}^{\mathcal{L}} \left(\sum_{n=1}^{\mathcal{N}} \|\mathbf{x}_i\|_2 \|\mathbf{w}_{m,n} - \tilde{\mathbf{w}}_{m,n}\|_2 \right)^2 \right) \\
&\leq \frac{1}{M} \sum_{i=1}^N \sum_{m=1}^M \left(\sum_{n=1}^{\mathcal{N}} \left(\left((\sqrt{\mathcal{L}} \|\boldsymbol{\theta} - \tilde{\boldsymbol{\theta}}\|_2 \alpha \|\mathbf{x}_i\|_2) + \left(2\alpha \|\mathbf{x}_i\|_2^2 \sqrt{\mathcal{N}} \|\boldsymbol{\theta} - \tilde{\boldsymbol{\theta}}\|_2 v \mathcal{L} \right) \right)^2 \right) \right. \\
&\quad \left. + \sum_{\ell=1}^{\mathcal{L}} \left(\sqrt{\mathcal{N}} \|\mathbf{x}_i\|_2 \|\boldsymbol{\theta} - \tilde{\boldsymbol{\theta}}\|_2 \right)^2 \right) \\
&\leq \sum_{i=1}^N \left(\mathcal{N} \left(\alpha \sqrt{\mathcal{L}} \|\mathbf{x}_i\|_2 + 2\alpha \|\mathbf{x}_i\|_2^2 \sqrt{\mathcal{N}} v \mathcal{L} \right)^2 + \mathcal{L} \mathcal{N} \|\mathbf{x}_i\|_2^2 \right) \|\boldsymbol{\theta} - \tilde{\boldsymbol{\theta}}\|_2^2. \tag{D.23}
\end{aligned}$$

By considering the square root of both sides in Equation (D.17) and Equation (D.23), we conclude the proof for Lemma 8. \square

E Details of numerical experiments

E.1 Setup

E.1.1 Dataset acquisition

We use the UCI datasets (Dua & Graff, 2017) preprocessed by Fernández-Delgado et al. (2014), which are publicly available at <http://persoal.citius.usc.es/manuel.fernandez.delgado/papers/jmlr/data.tar.gz>. Since the size of the kernel is the square of the dataset size and too many data make training impractical, we use preprocessed UCI datasets with the number of samples smaller than 5000. Arora et al. (2020) reported the bug in the preprocess when the explicit training/test split is given. Therefore, we do not use that dataset with explicit training/test split. As a consequence, 90 different datasets are available.

E.1.2 Kernel specifications

TNTK See Theorem 1 for the detailed definitions. We change the tree depth from 1 to 29 and change α in $\{0.5, 1.0, 2.0, 4.0, 8.0, 16.0, 32.0, 64.0\}$.

MLP-induced NTK We assume the MLP activation function as ReLU. Our implementation is based on the publicly available code⁴ used in Arora et al. (2020). For the detailed definitions, see Arora et al. (2020). The hyperparameter of this kernel is the model depth. We change the depth from 1 to 29. Here, depth = 1 means there is no hidden layer in the MLP.

RBF kernel We use scikit-learn implementation⁵. The hyperparameter of this kernel is γ , inverse of the standard deviation of the RBF kernel (Gaussian function). For Figure 3, we tune γ in $\{0.01, 0.02, 0.03, 0.04, 0.05, 0.06, 0.07, 0.08, 0.09, 0.1, 0.2, 0.3, 0.4, 0.5, 0.6, 0.7, 0.8, 0.9, 1.0, 2.0, 3.0, 4.0, 5.0, 6.0, 7.0, 8.0, 9.0, 10.0, 20.0, 30.0\}$, resulting in 30 candidates in total. In our experiments, $\gamma = 2.0$ performs the best on average (Figure 8).

E.1.3 Model specifications

We used kernel regression implemented in scikit-learn⁶. To consider ridge-less situation, regularization strength is set to be 1.0×10^{-8} , a very small constant.

⁴<https://github.com/LeoYu/neural-tangent-kernel-UCI>

⁵https://scikit-learn.org/stable/modules/generated/sklearn.metrics.pairwise.rbf_kernel.html

⁶https://scikit-learn.org/stable/modules/generated/sklearn.kernel_ridge.KernelRidge.html

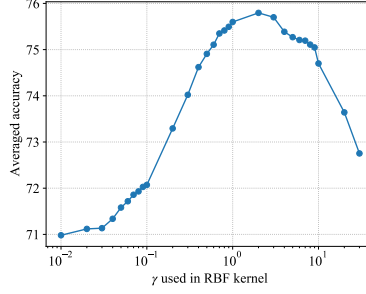


Figure 8: The γ dependency of the RBF kernel performance.

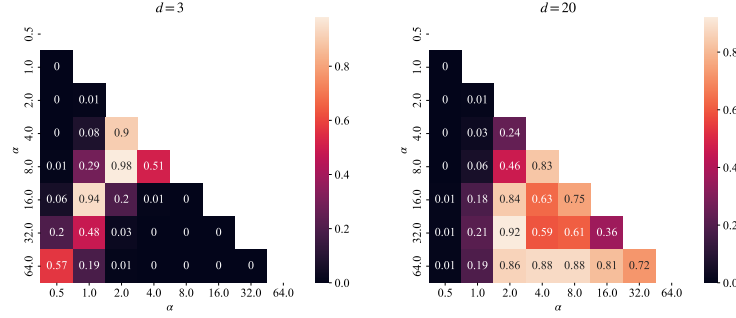


Figure 9: P-values of the Wilcoxon signed rank test for different pairs of α .

E.1.4 Computational resource

We used Ubuntu Linux (version: 4.15.0-117-generic) and ran all experiments on 2.20 GHz Intel Xeon E5-2698 CPU and 252 GB of memory.

E.2 Results

E.2.1 Statistical significance of the parameter dependency

Wilcoxon signed rank test is carried out to check the statistical significance of the differences between different α . Figure 9 shows the p-values for the depth of 3 and 20. As shown in Figure 6, when the tree is shallow, the accuracy started to deteriorate after around $\alpha = 8.0$, but as the tree becomes deeper, the deterioration became less apparent. Therefore, statistically significantly different pairs for deep trees and shallow trees are different. When the tree is deep, large α shows a significant difference over those with small α . However, when the tree is shallow, the best performance is achieved with α of about 8.0, and if α is too large, the performance deteriorates predominantly.

E.2.2 Dataset-wise results

For each α , scatter-plots are shown in Figures 10 and 11. As shown in Figure 12, the correlation coefficients with the TNTK are likely to be higher for the MLP-induced NTK compared to the RBF kernel. Tables 2, 3 and 4 are dataset-wise results of the comparison between the TNTK, the MLP-induced NTK, and the RBF kernel. For each α , depth is tuned for each dataset. In terms of the depth, the best performers from 1 to 29 are compared with the TNTK and the MLP-induced NTK. For the RBF kernel, γ is tuned in each dataset from 30 candidate values as described in Section E.1.2. Therefore, the number of tunable parameters is the same across all methods. All parameter-wise results are visualized in Figures 13 and 14.

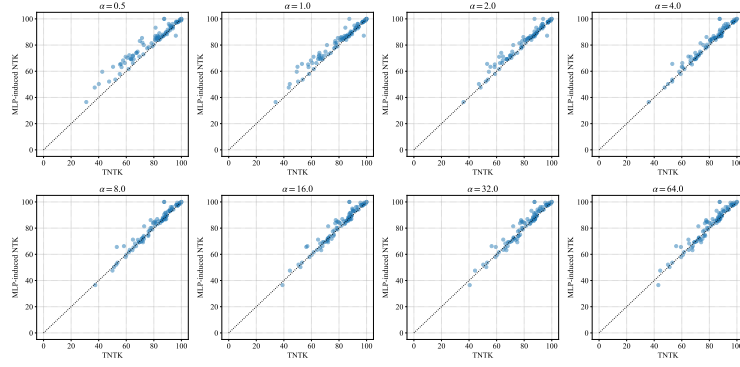


Figure 10: Performance comparisons between the kernel regression with MLP-induced NTK and the TNTK on the UCI dataset.

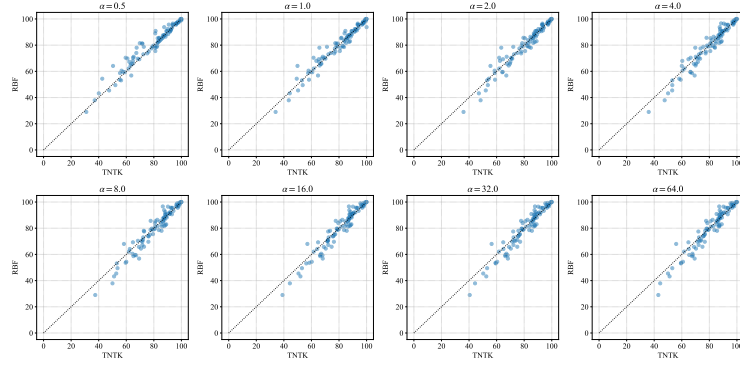


Figure 11: Performance comparisons between the kernel regression with RBF kernel and the TNTK on the UCI dataset.

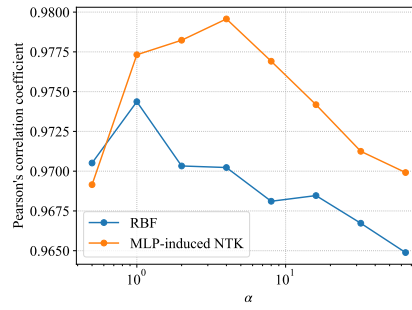


Figure 12: Pearson's correlation coefficients with predicted values of the TNTK with different α .

	name	size	$\alpha=0.5$	$\alpha=1.0$	$\alpha=2.0$	$\alpha=4.0$	$\alpha=8.0$	$\alpha=16.0$	$\alpha=32.0$	$\alpha=64.0$	MLP-NTK	RBF
0	trains	10	87.500	87.500	87.500	87.500	87.500	87.500	87.500	87.500	100.000	87.500
1	balloons	16	87.500	100.000	93.750	87.500	87.500	87.500	87.500	87.500	100.000	93.750
2	lenses	24	87.500	87.500	87.500	87.500	87.500	87.500	87.500	87.500	87.500	87.500
3	lung-cancer	32	56.250	53.125	53.125	53.125	53.125	56.250	59.375	59.375	65.625	53.125
4	post-operative	90	63.636	64.773	67.045	69.318	69.318	68.182	68.182	69.318	69.318	56.818
5	pittsburg-bridges-SPAN	92	55.435	57.609	58.696	67.391	65.217	66.304	66.304	67.391	65.217	58.696
6	fertility	100	84.000	88.000	89.000	89.000	89.000	89.000	89.000	89.000	89.000	83.000
7	zoo	101	100.000	99.000	99.000	99.000	99.000	99.000	99.000	99.000	99.000	99.000
8	pittsburg-bridges-T-OR-D	102	81.000	84.000	87.000	89.000	89.000	89.000	88.000	88.000	87.000	89.000
9	pittsburg-bridges-REL-L	103	67.308	74.038	75.000	74.038	75.962	75.962	75.962	75.962	74.038	74.038
10	pittsburg-bridges-TYPE	105	57.692	59.615	64.423	66.346	66.346	66.346	66.346	65.385	68.269	59.615
11	molec-biol-promoter	106	90.385	88.462	87.500	87.500	87.500	87.500	87.500	87.500	90.385	88.462
12	pittsburg-bridges-MATERIAL	106	93.269	94.231	94.231	94.231	94.231	94.231	94.231	94.231	94.231	93.269
13	breast-tissue	106	65.385	68.269	67.308	70.192	72.115	72.115	75.000	74.038	69.231	71.154
14	acute-nephritis	120	100.000	100.000	100.000	100.000	100.000	100.000	100.000	100.000	100.000	100.000
15	acute-inflammation	120	100.000	100.000	100.000	100.000	100.000	100.000	100.000	100.000	100.000	100.000
16	heart-switzerland	123	37.097	43.548	48.387	47.581	50.000	44.355	44.355	44.355	47.581	37.903
17	echocardiogram	131	81.061	81.061	84.848	84.091	85.606	85.606	85.606	85.606	85.606	78.030
18	lymphography	148	88.514	88.514	88.514	88.514	87.838	87.162	86.486	86.486	88.514	86.486
19	iris	150	95.946	97.973	96.622	88.514	86.486	87.162	87.838	87.162	87.162	96.622
20	teaching	151	56.579	57.895	58.553	60.526	64.474	67.105	67.105	67.763	63.158	60.526
21	hepatitis	155	83.974	85.256	85.256	84.615	84.615	84.615	84.615	85.256	83.974	85.256
22	wine	178	98.864	99.432	98.864	98.864	98.864	98.295	98.295	97.727	99.432	98.295
23	planning	182	62.222	65.556	70.000	71.667	71.667	72.222	72.222	72.222	72.222	67.222
24	flags	194	52.083	53.646	53.646	53.125	53.646	53.125	53.125	53.125	53.646	49.479
25	parkinsons	195	93.878	94.388	92.857	93.367	92.857	92.857	93.367	93.367	93.878	95.408
26	breast-cancer-wisc-prog	198	82.143	83.673	83.673	83.673	83.673	83.673	83.673	83.673	85.204	78.571
27	heart-va	200	31.000	34.000	36.000	36.000	37.500	39.000	40.500	43.000	36.500	29.000
28	conn-bench-sonar-mines-rocks	208	86.538	86.538	87.019	86.538	86.538	86.538	86.538	86.538	87.981	87.500
29	seeds	210	90.865	93.750	93.269	91.827	92.308	92.308	91.827	91.827	96.154	95.673

Table 2: Comparison between TNTK and MLP-induced NTK for a half of the dataset (1/3).

	name	size	$\alpha=0.5$	$\alpha=1.0$	$\alpha=2.0$	$\alpha=4.0$	$\alpha=8.0$	$\alpha=16.0$	$\alpha=32.0$	$\alpha=64.0$	MLP-NTK	RBF
30	glass	214	60.849	67.453	70.755	70.755	71.698	71.698	71.226	71.226	70.283	69.811
31	statlog-heart	270	83.209	87.313	87.687	88.433	88.433	88.433	87.687	87.313	86.567	82.463
32	breast-cancer	286	64.789	67.254	69.718	70.423	72.887	74.648	75.000	75.000	71.831	65.845
33	heart-hungarian	294	83.219	83.904	84.247	84.589	85.616	85.274	85.274	85.274	85.616	82.877
34	heart-cleveland	303	55.263	58.224	58.882	59.211	59.539	58.553	59.211	59.539	57.895	53.618
35	haberman-survival	306	59.539	61.513	61.842	66.447	68.421	71.711	73.684	73.684	71.053	70.395
36	vertebral-column-2classes	310	69.805	77.273	78.571	80.844	82.792	84.091	84.091	82.792	83.117	81.494
37	vertebral-column-3classes	310	71.753	78.247	81.169	80.844	80.844	81.818	81.494	81.169	81.818	81.169
38	primary-tumor	330	47.561	50.305	52.134	53.049	52.744	50.610	50.305	50.000	52.134	45.427
39	ecoli	336	71.429	79.167	83.036	84.524	86.012	86.607	86.905	86.905	85.417	81.250
40	ionosphere	351	90.057	91.477	90.341	87.784	88.352	88.352	88.352	88.352	91.761	92.330
41	libras	360	82.778	81.389	80.556	80.833	81.111	80.833	80.833	80.833	83.889	85.278
42	dermatology	366	97.802	97.802	97.527	97.527	97.253	97.253	97.253	97.253	97.802	97.253
43	congressional-voting	435	61.697	61.697	61.927	61.927	61.927	61.697	61.697	61.697	61.697	62.156
44	arrhythmia	452	69.469	65.265	64.602	64.823	64.823	64.823	64.823	64.823	71.239	69.248
45	musk-1	476	89.076	89.076	89.076	89.286	89.286	89.076	89.076	89.076	89.706	90.756
46	cylinder-bands	512	79.883	78.125	78.125	78.320	78.516	78.320	78.320	78.320	80.273	79.688
47	low-res-spect	531	91.729	91.353	90.602	89.474	88.534	87.782	87.218	87.218	91.353	90.226
48	breast-cancer-wisc-diag	569	96.127	96.655	97.359	97.359	97.359	96.831	96.479	96.479	97.007	95.599
49	ilpd-indian-liver	583	64.897	69.521	70.719	72.260	71.062	71.747	72.603	72.603	71.918	70.377
50	synthetic-control	600	99.333	99.333	99.167	98.833	98.333	97.833	97.000	96.667	98.833	99.333
51	balance-scale	625	81.250	84.615	88.782	89.904	91.346	90.064	85.256	85.256	93.269	90.865
52	statlog-australian-credit	690	59.012	60.610	64.099	66.279	67.151	68.023	68.023	68.023	66.279	59.302
53	credit-approval	690	82.558	85.174	86.628	87.209	87.645	87.791	87.791	87.355	87.064	81.686
54	breast-cancer-wisc	699	96.286	97.286	97.857	97.857	98.000	98.000	98.000	98.000	98.000	96.714
55	blood	748	67.513	65.775	63.369	69.786	72.727	73.529	75.802	77.005	74.064	78.075
56	energy-y2	768	89.583	89.453	88.021	87.891	88.151	87.630	87.630	87.630	88.281	90.755
57	pima	768	68.229	70.182	71.354	73.307	76.042	76.302	77.083	76.693	75.000	69.661
58	energy-y1	768	93.750	93.620	93.229	90.495	90.234	90.104	90.234	90.234	92.708	96.484
59	statlog-vehicle	846	78.318	77.014	76.540	73.578	72.986	72.156	72.038	72.038	81.398	77.488

Table 3: Comparison between TNTK and MLP-induced NTK for a half of the dataset (2/3).

	name	size	$\alpha=0.5$	$\alpha=1.0$	$\alpha=2.0$	$\alpha=4.0$	$\alpha=8.0$	$\alpha=16.0$	$\alpha=32.0$	$\alpha=64.0$	MLP-NTK	RBF
60	oocytes_trisopterus_nucleus_2f	912	82.456	82.566	82.456	82.675	80.811	78.728	78.070	77.851	84.978	79.605
61	oocytes_trisopterus_states_5b	912	92.325	92.982	93.640	93.092	91.667	90.022	89.693	89.693	94.189	91.228
62	tic-tac-toe	958	99.268	99.163	99.268	99.268	99.268	99.268	99.268	99.268	98.640	100.000
63	mammographic	961	72.708	71.250	72.083	75.625	77.604	78.854	78.958	79.271	80.000	78.750
64	statlog-german-credit	1000	75.200	76.500	77.800	77.300	76.200	75.500	75.500	75.400	77.500	73.700
65	led-display	1000	72.400	72.300	72.600	72.500	72.300	72.500	72.300	72.500	72.900	73.000
66	oocytes_merluccius_nucleus_4d	1022	81.078	80.588	80.686	80.686	79.412	77.255	76.961	76.765	83.725	75.490
67	oocytes_merluccius_states_2f	1022	92.353	91.961	92.157	92.157	91.373	90.784	90.784	90.490	93.039	92.059
68	contrac	1473	40.082	44.293	47.147	50.068	51.155	52.038	52.514	51.155	50.272	43.207
69	yeast	1484	42.588	49.326	54.380	58.154	60.040	60.243	60.445	60.849	59.636	54.380
70	semeion	1593	93.719	93.467	93.405	93.467	93.467	93.467	93.467	93.405	96.168	95.603
71	wine-quality-red	1599	63.062	65.938	68.812	70.000	70.625	70.375	70.312	70.312	69.625	64.438
72	plant-texture	1599	83.812	81.812	79.438	77.938	77.688	77.625	77.750	77.625	86.125	85.625
73	plant-margin	1600	84.750	83.938	82.938	81.875	80.750	79.500	78.938	78.563	84.875	83.875
74	plant-shape	1600	64.812	63.562	62.438	60.375	58.312	57.062	56.375	55.937	66.250	68.000
75	car	1728	97.454	97.569	97.164	96.701	96.354	96.181	96.123	96.123	97.743	98.032
76	steel-plates	1941	76.289	77.320	77.938	77.423	77.062	76.753	76.598	76.495	78.351	75.103
77	cardiotocography-3clases	2126	92.232	92.514	92.043	91.902	91.949	91.855	91.996	91.855	93.173	92.043
78	cardiotocography-10clases	2126	80.838	82.957	82.250	80.744	79.896	79.896	79.661	79.614	84.181	79.143
79	titanic	2201	78.955	78.955	78.955	78.955	78.955	78.955	78.955	78.955	78.955	78.955
80	statlog-image	2310	96.360	96.967	97.097	96.750	96.231	95.927	95.884	95.624	97.660	96.404
81	ozone	2536	97.358	97.240	97.200	97.200	97.200	97.200	97.200	97.200	97.397	97.200
82	molec-biol-splice	3190	86.731	85.947	84.536	83.093	82.465	82.403	82.371	82.371	86.920	86.418
83	chess-krvkp	3196	99.124	98.905	98.655	97.872	96.902	95.526	95.307	95.307	99.406	98.999
84	abalone	4177	50.407	49.880	55.532	60.010	62.548	64.200	64.943	65.086	63.410	64.152
85	bank	4521	88.628	89.336	89.358	89.513	89.358	89.159	89.181	89.159	89.735	88.142
86	spambase	4601	91.478	91.174	92.435	90.652	93.130	89.630	91.478	93.348	94.913	90.652
87	wine-quality-white	4898	63.623	66.810	67.545	68.791	69.158	68.975	68.995	68.913	69.097	65.748
88	waveform-noise	5000	86.360	86.340	86.520	86.540	86.720	86.500	85.900	85.520	86.540	85.460
89	waveform	5000	85.440	85.780	86.300	86.500	86.660	86.700	86.740	86.520	86.340	84.640

Table 4: Comparison between TNTK and MLP-induced NTK for a half of the dataset (3/3).

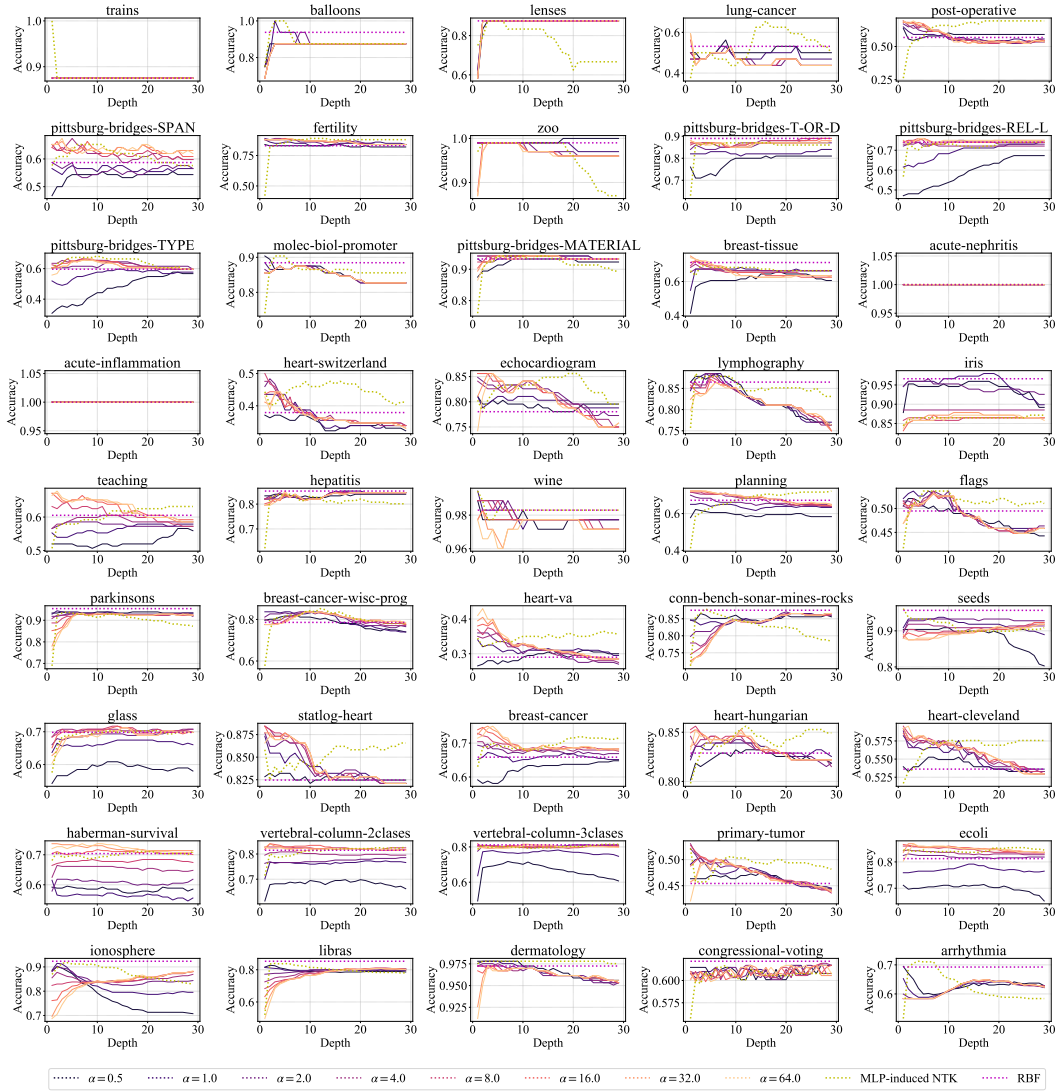


Figure 13: Dataset-wise comparison for a half of the dataset (1/2).

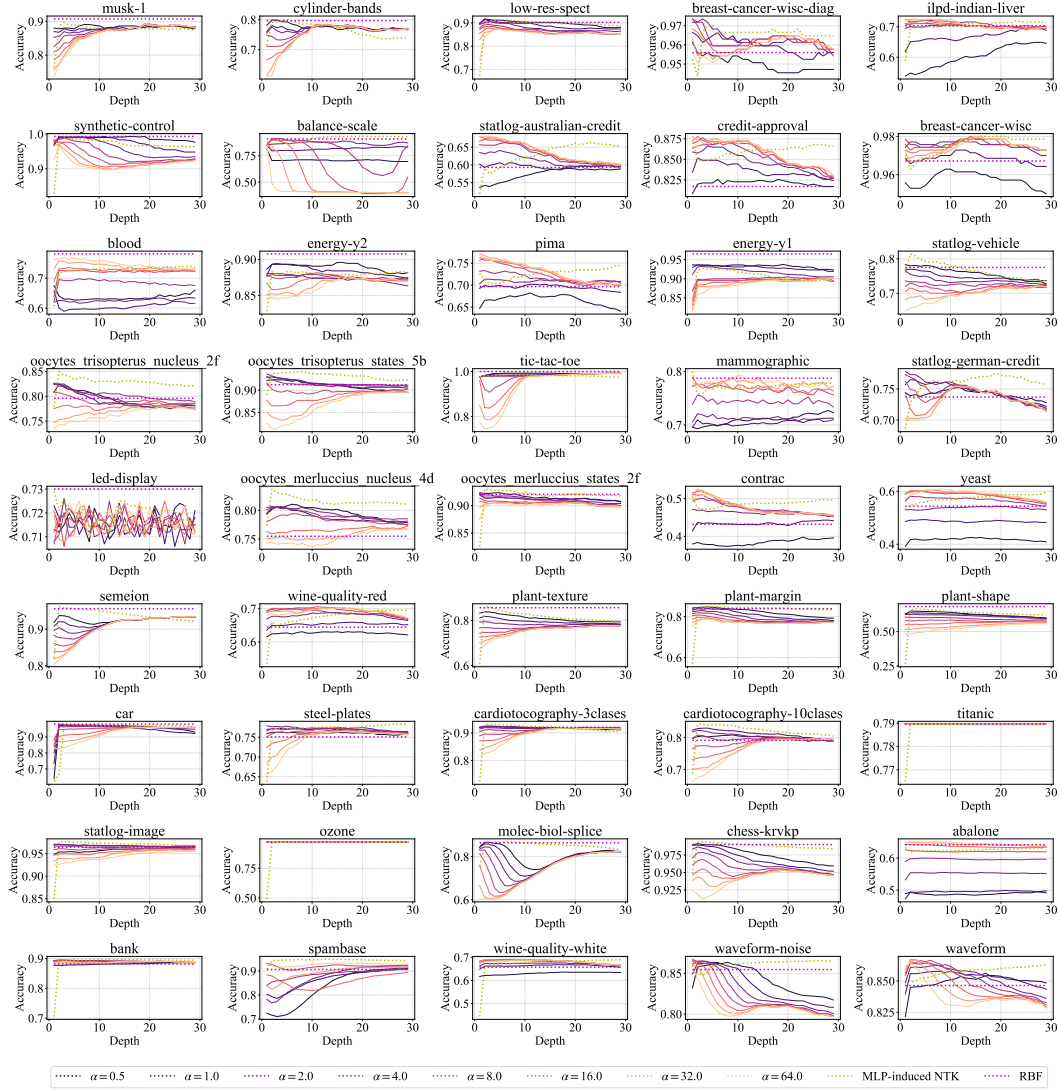


Figure 14: Dataset-wise comparison for a half of the dataset (2/2).